cmgh
CELLULAR AND MOLECULAR GASTROENTEROLOGY AND HEPATOLOGY

ORIGINAL RESEARCH

Oxidized Low-Density Lipoprotein Drives Dysfunction of the Liver Lymphatic System

Matthew A. Burchill,[1,2] Jeffrey M. Finlon,[1,*] Alyssa R. Goldberg,[1,3,*] Austin E. Gillen,[2,4] Petra A. Dahms,[1] Rachel H. McMahan,[5] Anne Tye,[1] Andrew B. Winter,[6] Julie A. Reisz,[4] Eric Bohrnsen,[4] Johnathon B. Schafer,[1] Angelo D'Alessandro,[4] David J. Orlicky,[7] Michael S. Kriss,[1] Hugo R. Rosen,[8] Rebecca L. McCullough,[6] and Beth A. Jirón Tamburini[1,2,9]

[1]Division of Gastroenterology and Hepatology, University of Colorado Anschutz Medical Campus, Aurora, Colorado; [2]RNA Biosciences Initiative, University of Colorado Anschutz Medical Campus, Aurora, Colorado; [3]Section of Pediatric Gastroenterology, Hepatology and Nutrition, Children's Hospital Colorado, University of Colorado Anschutz Medical Campus, Aurora, Colorado; [4]Department of Biochemistry and Molecular Genetics, University of Colorado Anschutz Medical Campus, Aurora, Colorado; [5]Department of Surgery, University of Colorado Anschutz Medical Campus, Aurora, Colorado; [6]Department of Pharmacology, University of Colorado Anschutz Medical Campus, Aurora, Colorado; [7]Department of Pathology, University of Colorado Anschutz Medical Campus, Aurora, Colorado; [8]University of Southern California Keck School of Medicine, Los Angeles, California; and [9]Department of Immunology and Microbiology, University of Colorado Anschutz Medical Campus, Aurora, Colorado

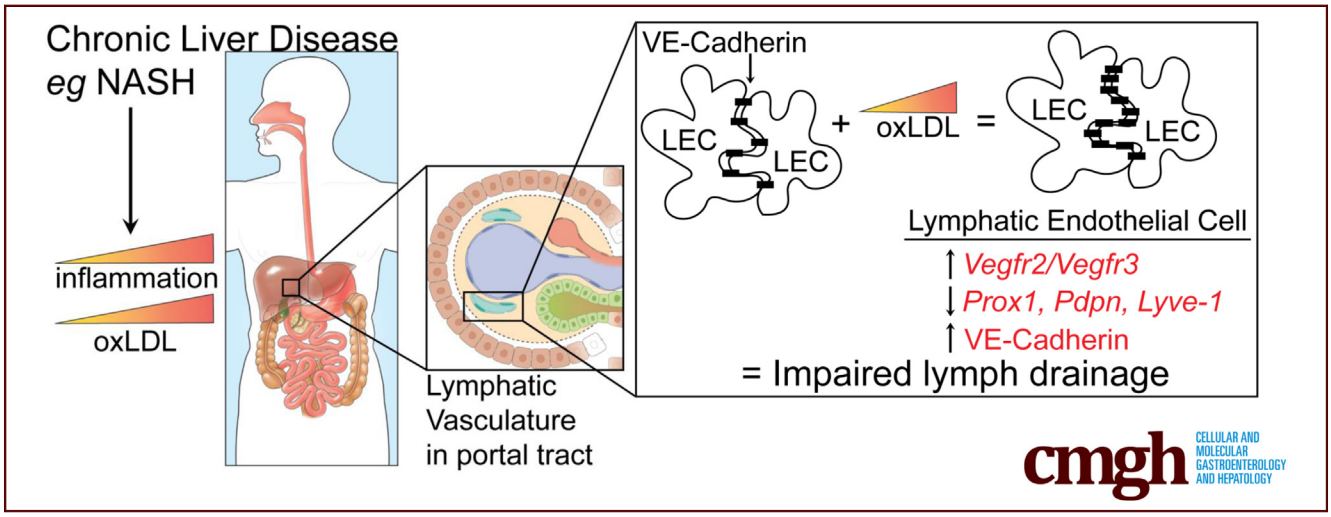

SUMMARY

Chronic liver disease results in lymphatic dysfunction in the liver which is rescued by administration of recombinant vascular endothelial growth factor C. The lymphatic dysfunction causes a decrease in lymphatic transport of molecules and occurs via oxidized LDL dependent loss of lymphatic identity.

BACKGROUND AND AIMS: As the incidence of nonalcoholic steatohepatitis (NASH) continues to rise, understanding how normal liver functions are affected during disease is required before developing novel therapeutics which could reduce morbidity and mortality. However, very little is understood about how the transport of proteins and cells from the liver by the lymphatic vasculature is affected by inflammatory mediators or during disease.

METHODS: To answer these questions, we utilized a well-validated mouse model of NASH and exposure to highly oxidized low density lipoprotein (oxLDL). In addition to single cell sequencing, multiplexed immunofluorescence and metabolomic analysis of liver lymphatic endothelial cells (LEC)s we evaluated lymphatic permeability and transport both in vitro and *in vivo*.

RESULTS: Confirming similarities between human and mouse liver lymphatic vasculature in NASH, we found that the lymphatic vasculature expands as disease progresses and results in the downregulation of genes important to lymphatic identity and function. We also demonstrate, in mice with NASH, that fluorescein isothiocyanate (FITC) dextran does not accumulate in the liver draining lymph node upon intrahepatic

injection, a defect that was rescued with therapeutic administration of the lymphatic growth factor, recombinant vascular endothelial growth factor C (rVEGFC). Similarly, exposure to oxLDL reduced the amount of FITC-dextran in the portal draining lymph node and through an LEC monolayer. We provide evidence that the mechanism by which oxLDL impacts lymphatic permeability is via a reduction in *Prox1* expression which decreases lymphatic specific gene expression, impedes LEC metabolism and reorganizes the highly permeable lymphatic cell-cell junctions which are a defining feature of lymphatic capillaries.

CONCLUSIONS: We identify oxLDL as a major contributor to decreased lymphatic permeability in the liver, a change which is consistent with decreased protein homeostasis and increased inflammation during chronic liver disease. *(Cell Mol Gastroenterol Hepatol 2021;11:573–595; https://doi.org/10.1016/j.jcmgh.2020.09.007)*

Keywords: Oxidized LDL; Lymphangiogenesis; VEGFC; Permeability; Inflammation.

Currently, in the United States, ~17,000 people are on the liver transplant waiting list and only 38% of those people will receive a transplant due to organ shortage (Organ Procurement and Transplant Network data as of 2019). The number of people on the waiting list is projected to increase by 23% in the next 15 years, with nonalcoholic steatohepatitis (NASH) projected to become the leading indication for liver transplantation in the United States.[1,2] The current health care expenditure associated with liver transplantation is approximately $1.43 million per patient, which will increase to $2.1 million in the next 15 years. These data highlight the need for alternative treatment options for patients with chronic liver disease. Thus, the development of novel targets and therapeutic options for patients that currently have none is needed.

The liver lymphatic system, while largely understudied, holds an essential role in organ health. The primary function of the lymphatic system is to transport interstitial fluid (lymph) from the tissue to the circulatory system for removal from the body.[3] The lymphatics also participate in the transport of proteins and lipoproteins to maintain protein homeostasis[4] and trafficking of tissue resident immune cells such as dendritic cells to the lymph node (LN).[5] Previous studies spanning the years of 1960–1985 demonstrated that during cirrhosis, the lymph draining from the liver is depleted of high-molecular-weight proteins in both human and animal models.[6–8] These studies postulated that low lymph protein content in cirrhosis was a result of decreased permeability of the microvascular system. However, this interpretation was limited by the tools available at the time, and thus how lymphatic or vascular permeability contributed to these differences was unknown. Since 1985, new markers and regulators of the lymphatics have been discovered. One of these regulators is PROX1, a transcription factor required for lineage commitment of lymphatic endothelial cells (LECs),[9,10] which regulates the expression of other lymphatic markers including podoplanin (PDPN), lymphatic vessel endothelial receptor 1 (LYVE-1),[11] and vascular endothelial growth factor receptor 3 (VEGFR3).[12] In the last 35 years, these markers have allowed investigators to distinguish between blood and lymphatic vasculature and develop assays to model LEC signaling pathways and specific LEC functions that occur in vivo.[13–16] Perhaps one of the most striking findings in the last 15 years was the discovery of the functionally specialized button-like junctions in LECs found in the lymphatic capillaries.[17] These button junctions allow for cells and proteins to pass freely from the tissue into the lymph for immune surveillance in the LN.[18] Whether these lymphatic functions are required in the liver to mitigate inflammation is unknown and has been largely overlooked, particularly in the setting of chronic liver diseases, such as NASH.

While oxidized low-density lipoprotein (oxLDL) is a key player in the pathogenesis of atherosclerosis,[19] mounting evidence suggests that oxLDL can contribute to the progression of liver disease.[20,21] OxLDL accumulates as a result of free radicals generated by inflammation and can directly induce liver injury.[22] Further, levels of oxLDL are elevated in the serum of patients with NASH,[23] hepatitis C infection,[24] alcoholic liver disease,[25] and cholestasis.[26] Antibodies specific to oxLDL may be a biomarker for people with underlying NASH[23] and neutralization of oxLDL ameliorates experimental nonalcoholic fatty liver disease (NAFLD), a precursor to NASH, in mice.[27] Finally, lipid lowering medication has been demonstrated to reduce liver inflammation in both mice and humans.[28–30] These findings point to oxLDL as being an important mediator in the progression of chronic liver disease, however the precise mechanism(s) by which oxLDL influences liver inflammation is unknown.

In this study, we demonstrate in both people and mice with fatty liver disease that the lymphatic system draining the liver is significantly altered. Specifically, using single-cell sequencing, we demonstrate that LECs from a diseased liver have a significant reduction of transcripts that are associated with LEC identity and function. Further, we find defects in the ability of the lymphatic vasculature to properly

***Authors contributed equally.**

Abbreviations used in this paper: **ALT, alanine aminotransferase; AST, aspartate aminotransferase; BSA, bovine serum albumin; CK19, cytokeratin-19; FAO, fatty acid oxidation; FITC, fluorescein isothiocyanate; HFHC, high fat, high cholesterol; hLEC, human lymphatic endothelial cell; HRP, horseradish peroxidase; HUVEC, human primary umbilical vein endothelial cell; LEC, lymphatic endothelial cell; LN, lymph node; LSEC, liver sinusoidal endothelial cell; LVD, lymphatic vessel density; LYVE-1, lymphatic vessel endothelial receptor 1; NAFLD, nonalcoholic fatty liver disease; NASH, nonalcoholic steatohepatitis; OxLDL, oxidized low density lipoprotein; PBS, phosphate-buffered saline; PDPN, podoplanin; PEC, portal endothelial cell; RT-qPCR, reverse-transcription quantitative polymerase chain reaction; TBST, Tris-buffered saline with 0.1% Tween 20 detergent; VEGFC, vascular endothelial growth factor C; VEGFR3, vascular endothelial growth factor receptor 3.**

Most current article

2352-345X
https://doi.org/10.1016/j.jcmgh.2020.09.007

transit fluorescein isothiocyanate (FITC) dextran to the portal lymph node during disease. A finding which can be rescued by treatment with a lymphatic growth factor, vascular endothelial growth factor C (VEGFC). We identify significant alterations in LECs in the presence of oxLDL, an inflammatory mediator of fatty liver disease, including changes in transcription, metabolism and permeability. Finally, we demonstrate defects in FITC-dextran transport from the liver to the portal LN could be directly induced by systemic treatment with oxLDL, an effect that was independent of liver inflammation. Together, these data combined with published findings provide evidence that protein homeostasis, maintained by lymphatic vasculature, is compromised in mice and people with NASH, that oxLDL may be a significant contributing factor to this dysfunction, and that therapeutically targeting the lymphatic vasculature during disease could provide relief from chronic liver inflammation and ameliorate disease.

Results

The Lymphatic Vasculature Increases in the Liver During the Progression of NAFLD and NASH

Our previous publication demonstrated that lymphatic vessels were significantly expanded in the liver during cirrhosis, independent of disease etiology.[31] However, it was unclear if the liver lymphatic vasculature expanded during the progression of disease or if this lymphatic expansion was merely a consequence of changes in the liver associated with cirrhosis. To answer this question, we examined the lymphatic vessel density (LVD) of the lymphatic vasculature in portal and fibrotic regions of livers. We assessed biopsies from 45 individuals with various stages of NAFLD and NASH who received liver biopsy during elective gastric bypass surgery or who were referred to our hepatology clinic with a preliminary diagnosis of NASH (Table 1). Prior to inclusion in our study, patient biopsies were staged for fibrosis utilizing Brunt staging by a pathologist blinded to other clinical parameters. Using this patient cohort, we found that the lymphatic vasculature in the human liver expands with the progression of disease as measured by PDPN staining (Figure 1*A*) and quantified based on lymphatic area divided by tissue area (density) (Figure 1*B*). These findings demonstrate that the liver lymphatic vasculature significantly increases in parallel with the progression of disease and the observed expansion of the liver lymphatic vasculature during end-stage liver disease is not merely a consequence of cirrhosis.

A Murine Model of NASH Induced Liver Lymphangiogenesis and Reduced Lymphatic Marker Expression. The previous findings demonstrate that the lymphatic vasculature expands in the human liver during disease. To validate that similar processes occur in murine models of chronic liver disease, we stained numerous murine models of liver disease with PDPN, LYVE-1, and cytokeratin-19 (CK19). Similar to our findings in human disease, we found that the lymphatic vasculature expands in a murine model of NASH, defined as PDPN+LYVE-1+CK19– lymphatic vasculature and not PDPN+LYVE-1-CK19+ cholangiocytes (Figure 2*A* and *B*). As with our studies of human disease, the lymphatic expansion was caused by division of lymphatic endothelial cells over time, as we observed an increase in the frequency of Ki67+ lymphatic vasculature as disease progresses (Figure 2*C*). To better understand the effect of NASH on liver lymphatics, we used an established high-fat, high-cholesterol (HFHC) diet (45% fat and 2% cholesterol).[32] We chose a diet high in cholesterol, as our previous findings demonstrated that cholesterol caused a significant decline in the expression of lymphatic lineage–specific genes, *PROX1* and *FLT4/VEGFR3,* and led to impaired stability of lymphatic vessel like structures in vitro.[31] Upon staining of the HFHC livers we noticed the mean fluorescence intensity of both PDPN and LYVE-1 was decreased in the lymphatic vasculature (Figure 2*D*) consistent with in vitro data demonstrating that *Prox1*, a regulator of these genes, was downregulated when exposed to oxLDL.[31] Additionally, this increase of lymphatic density in murine livers during disease was independent of disease etiology (*MDR2–/–*, Lieber-DeCarli diet and high-fat,

Table 1. Patient Demographics

	F0 (n = 7)	F1 (n = 9)	F2 (n = 9)	F3 (n = 10)	F4 (n = 9)	*P* Value
Age, y	39 ± 13	48 ± 11	52 ± 14	49 ± 6	55 ± 12	.062[a]
Sex						.722
Female	3 (43)	4 (44)	4 (44)	7 (70)	4 (44)	
Male	4 (57)	5 (56)	5 (56)	3 (30)	5 (56)	
Race						
White/Caucasian	7	9	9	8	9	.999
African American	0	0	0	1	0	
Other	0	0	0	1	0	
Ethnicity						
Non-Hispanic	6	8	6	9	5	.155
Hispanic	1	1	3	0	4	
Other	0	0	0	1	0	

Values are mean ± SD, n (%), or n.
[a]F0 vs F4 was significant ($P = .0471$), all other pairwise comparisons were nonsignificant (Kruskal-Wallis); others are Fisher's exact test.

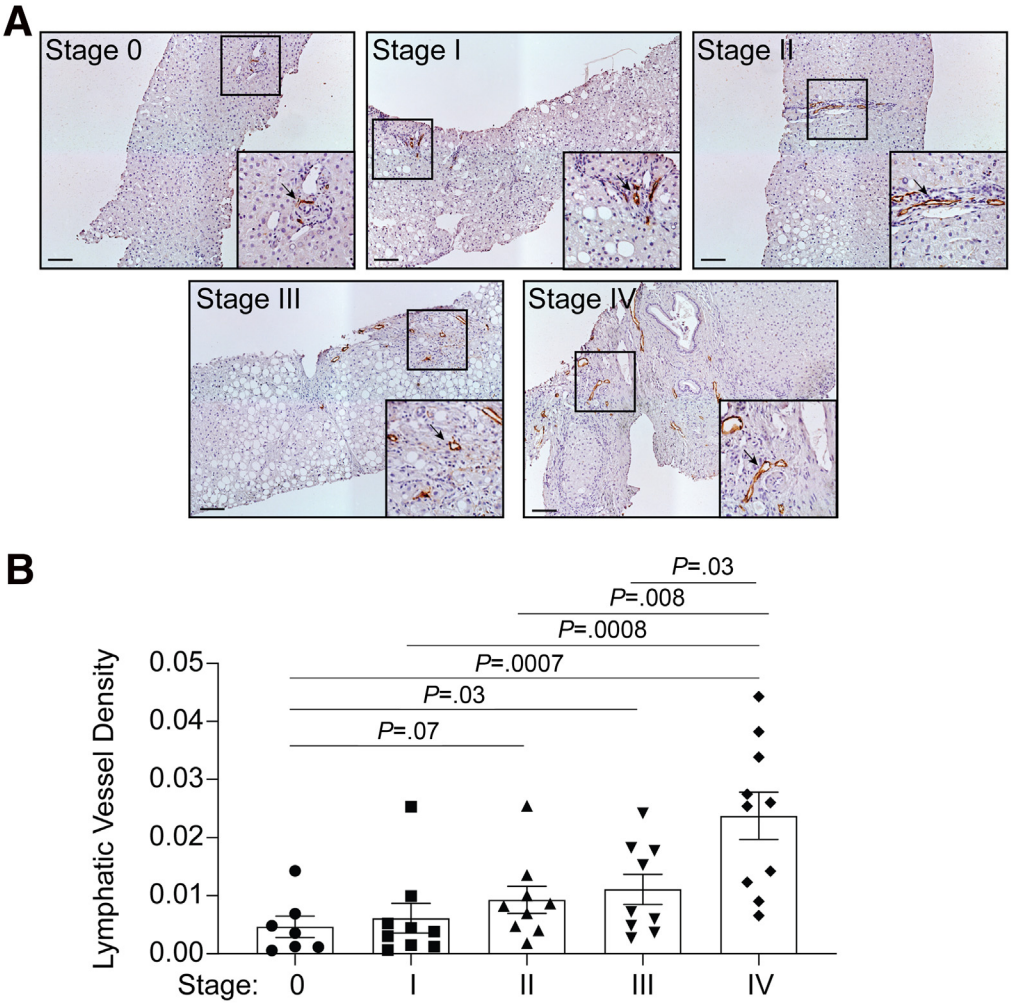

Figure 1. LVD increases as patients progress through stages of NASH. (*A*) Representative images of biopsies from patients in Table 1 ranging from stage 0 to IV of fibrosis using the Brunt staging method. Histological sections were stained with the PDPN (D2-40) antibody and visualized with DAB (brown). Sections were then counterstained with hematoxylin to visualize nuclei. Scale bar is 100 μm. Inset is the indicated zoomed in region. Arrows point to representative lymphatic vessels. (*B*) Lymphatic vessel density (area of the lymphatics divided by the area of the defined tissue area) based on areas of fibrosis were evaluated from 7 to 10 patients per stage. *P* values were calculated using a 1-way analysis of variance. Actual *P* values are shown.

low-cholesterol diet) (Figure 2*E* and *F*).[33] Using the HFHC diet model, we found that after 17–24 weeks on the diet, the mice developed steatosis and inflammation, increased aspartate aminotransferase (AST) and alanine aminotransferase (ALT), and increased total cholesterol, high-density lipoprotein, and LDL (Figure 3*A–D*). As our model of NASH demonstrates high liver LDL levels, these findings are also consistent with increased LDL exposure causing lymphatic-specific gene downregulation (Figure 2*D*). Finally, VEGFC transcript was increased in the liver, suggesting that the lymphatic expansion observed was caused by VEGFR3 engagement on the lymphatic vasculature (Figure 3*E*). Together, these data demonstrate that murine models of chronic liver disease can accurately recapitulate the lymphatic changes we find in human LECs exposed to cholesterol and in human chronic liver disease.

Chronic HFHC Diet Feeding Induces Transcriptional Changes in LECs. To determine if diet-induced liver disease, using our NASH model, alters the transcriptional profile of the lymphatic vasculature in the absence of cirrhosis, we utilized single-cell messenger RNA sequencing to determine differences in LEC transcriptional profile. Specifically, age-matched male mice were fed either a chow or HFHC diet for 22–32 weeks, and endothelial cells were enriched via flow cytometric sorting (Figure 4*A*). Sorted endothelial cells were then subjected to single cell sequencing as described.[31] LECs from control-fed mice were first clustered using clusifyr and then validated by canonical LEC gene expression such as *Lyve-1*, *Pdpn*, *Flt4*/*Vegfr3*, and *Prox1* (Figure 4*B*). Upon unsupervised clustering of the endothelial cells in the liver, we found that LECs and portal endothelial cells (PECs) cluster similarly to our human studies,[31] while liver sinusoidal endothelial cells (LSECs) are slightly more transcriptionally different than LEC or PECs (Figure 4*C*). This unbiased clustering allows us to

compare the transcriptional profiles of the LECs isolated from control- and HFHC-fed mice independent of the other cell types captured (Figures 4*D* and 5). Upon comparison of control LECs to HFHC LECs, we found significant disease pathways upregulated in LECs from the HFHC-fed mice. Using Ingenuity software analysis

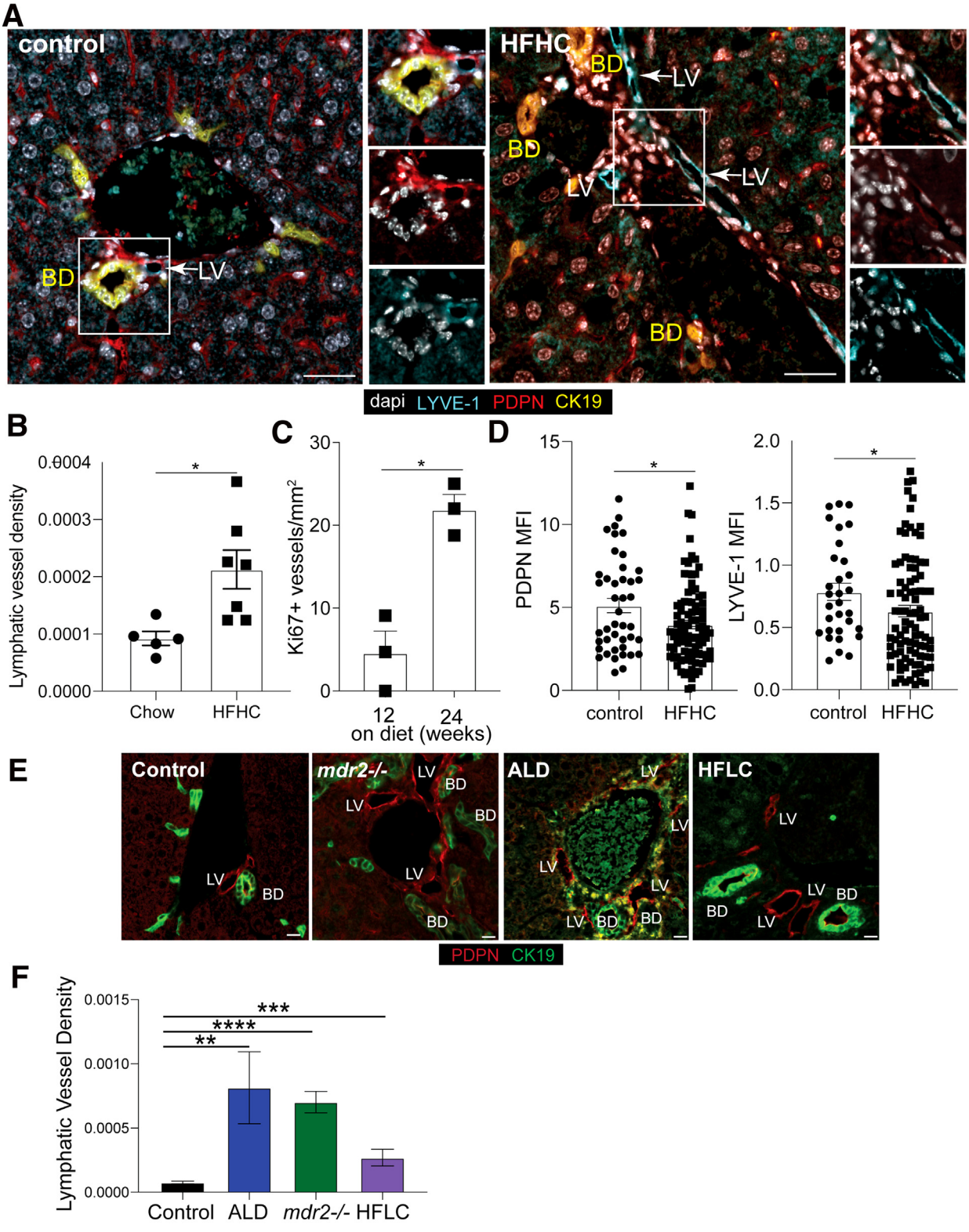

(IPA version 52921811; Qiagen, Germantown, MD), we discovered significant upregulation of catabolism, protein synthesis, interactions and binding of endothelial cells, lipid synthesis, and fatty acid metabolism among others (Figure 4*D*). When looking at differences in specific gene regulation, in control- vs HFHC-fed LECs, we evaluated LEC specific genes, genes involved in interactions and binding of endothelial cells, or lipid synthesis and fatty acid metabolism based on our pathway analysis. Upon evaluation of LEC specific genes, we saw a striking downregulation of *Lyve-1*, *Pdpn*, and *Prox1* in HFHC-fed mice (Figure 5*A*), consistent with our immunofluorescence staining of PDPN and LYVE-1 protein (Figure 2*D*) and the downregulation of *Prox1* in LECs exposed to oxLDL.[31] These changes were specific to LECs in the liver as the transcriptional profiles of either LSECs (Figure 5*B*) or PECs (Figure 5*C*) did not indicate an upregulation of VEGFR2 (*Kdr*), downregulation of VEGFR3 (*Flt4*), or an upregulation of VE-cadherin (*Cdh5*). Furthermore, the ratio between *Vegfr2* and *Vegfr3*, thought to be important for regulating permeable button-like structures between LECs,[34] was different in HFHC-fed compared with control-fed mice (Figure 5*D*). When evaluating genes involved in interactions and binding of endothelial cells, we saw little difference in LEC expression of integrin alpha 9 (*Itga9*); however VE-cadherin (*Cdh5*) expression appeared to be increased in diseased LECs (Figure 5*A*). Also consistent with increased lipid synthesis in LECs we observed an increase in expression of CD36, a gene also shown to be increased in response to oxLDL[35] as well as in liver LECs from individuals with NASH.[31] Finally, the proportion of LECs in active cell cycle (S/G2M), based on a defined set of genes known to regulate different stages of the cell cycle, was increased in HFHC-fed mice (Figure 5*E*), consistent with our findings in humans with NASH[31] and our Ki67 staining (Figure 2*C*). As we saw *VegfC* transcript upregulation using whole-liver reverse-transcription quantitative polymerase chain reaction (RT-qPCR) (Figure 3*E*) we asked about *VegfC* expression by the cell types we evaluated. We found that of the cell types we collected, LSECs and PECs were the primary source of *VegfC* in the liver (Figure 5*F*). However, as we sorted for endothelial cells, our data do not rule out *VegfC* expression by other cell types not collected in this analysis. In summary, the transcriptional profile of LECs from HFHC livers was consistent with changes in the LEC transcriptome that reflect both proliferation and a potential de-differentiation of liver LECs in the context of disease, which may impact their functions, such as permeability and metabolism.

Recombinant VEGFC (cys156ser) Promotes Lymphangiogenesis of LECs of the Liver

Access to the prolymphangiogenic cytokine, VEGFC, has been shown to promote lymphatic function,[36] the expression of *Prox1*,[37] and thus *Vegfr3*.[37,38] Because we found a decrease in *Vegfr3* expression by LECs in the HFHC diet we assessed if treating mice with rVEGFC (cys156ser) could promote lymphatic growth and differentiation. rVEGFC containing the cys156ser mutation selectively binds VEGFR3 homodimers found predominantly on lymphatic vessels.[39,40] LSECs, the primary endothelial cell found in the liver, express both VEGFR2 and VEGFR3 but in the form of a VEGFR2/3 heterodimer and utilize VEGFR2 for regeneration.[41] Thus, we asked if the cys156ser rVEGFC protein caused increased division of the LECs. We confirmed that rVEGFC (cys156ser) treatment resulted in increased lymphangiogenesis by quantification of the LVD in livers of treated mice (Figure 6*A* and *B*). This was in contrast to cholangiocytes, which also express VEGFR3 and do not change in frequency with rVEGFC (cys156ser) but do increase in frequency in the liver of HFHC mice (Figure 6*C*). Indeed, the injection of rVEGFC (cys156ser) to mice fed the HFHC diet for 3 weeks resulted in a significant increase in the frequency of Ki67+ LECs in the liver, but not Ki67+ LSECs (Figure 6*D*). While the rVEGFC (cys156ser) was specific to LEC proliferation and not LSEC proliferation we cannot rule out the possibility that the rVEGFC could affect other LSECs functions.

HFHC Diet Results in Defective Lymphatic Function in the Liver, Which Can Be Rescued by Administration of Recombinant VEGFC (cys156ser)

We observed lymphangiogenesis during disease progression in both humans (Figure 1) and mice (Figure 2), a transcriptional profile of liver LECs that was consistent with a loss of lymphatic identity (Figures 4 and 5), and lymphangiogenesis in the liver in response to rVEGFC (cys156ser). Therefore, we predicted that lymphatic

Figure 2. (***See previous page***). **Liver lymphatic vessels increase in frequency during disease.** (*A*) Mice were fed a control or HFHC diet for 24 weeks. Staining of liver sections was performed with DAPI (white), LYVE-1 (cyan), PDPN 8.8.1 (red), and CK19 (yellow). Scale bar is 100 μm. Shown is a representative image from 1 experiment with 5–7 mice per group repeated 2 additional times with similar results and statistical values. (*B*) Lymphatic vessels were designated as PDPN+CK19– structures with at least 2 nuclei per vessel. LVD was calculated as described in the Materials and Methods. (*C*) Number of Ki67+ lymphatic vessels per area of tissue over a 12-week to 24-week period. Few to no Ki67+ lymphatic vessels were detected prior to feeding HFHC diet. Three mice per time point were evaluated. Experiment was repeated with similar results. (*D*) Mean fluorescence intensity as a measure of protein levels of PDPN and LYVE-1 using inform software in indicated group acquired from images in panels *A* and *B*. (*E*) Staining and quantification of liver sections from control, 12-week-old *mdr2*–/– mice (a model of primary sclerosing cholangitis) and mice gavaged with ethanol (2% v/v) for 5 weeks (Lieber-DeCarli diet model). Sections were stained with PDPN, CK19, and DAPI. Scale bar is 20 μm. Statistical analysis was performed using an unpaired *t* test in which $^{*}P < .05$. $^{**}P < .01$, and $^{***}P < .001$. ALD, alcoholic liver disease; BD, bile duct; LV, lymphatic vessel.

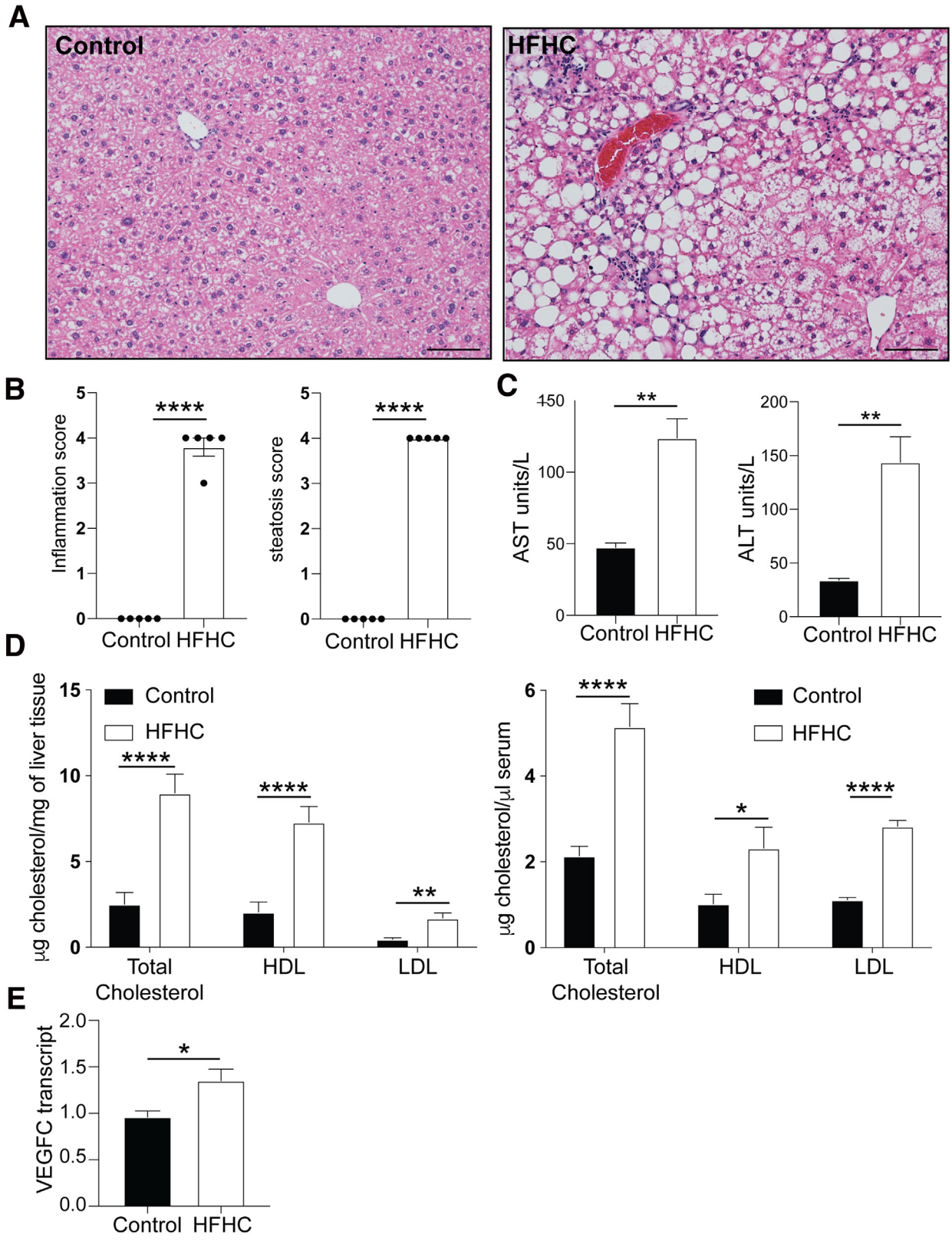

Figure 3. HFHC diet induces liver disease and increases cholesterol levels in mice. (*A*) Representative hematoxylin and eosin staining from control mice or mice fed an HFHC diet for 17 weeks (HFHC: 60% fat and 2% cholesterol). Scale bar is 20 μm. (*B*) Inflammation score (left) and steatosis score (right) for control or HFHC diet–fed mice. (*C*) Analysis of AST or ALT levels in the serum of mice fed either a control or HFHC diet for 17 weeks. (*D*) Quantitation of high-density lipoprotein (HDL), LDL, and total cholesterol (free and cell associated) by enzyme-linked immunosorbent assay from the liver or serum of mice fed a control or HFHC diet. (*E*) Whole-liver RT-qPCR of VEGFC transcript from control of HFHC diet. Shown are data from 1 independent experiment repeated at least 3 additional times. Statistical analysis was performed using an unpaired *t* test in which $^{*}P < .05$, $^{**}P < .01$, and $^{****}P < .001$.

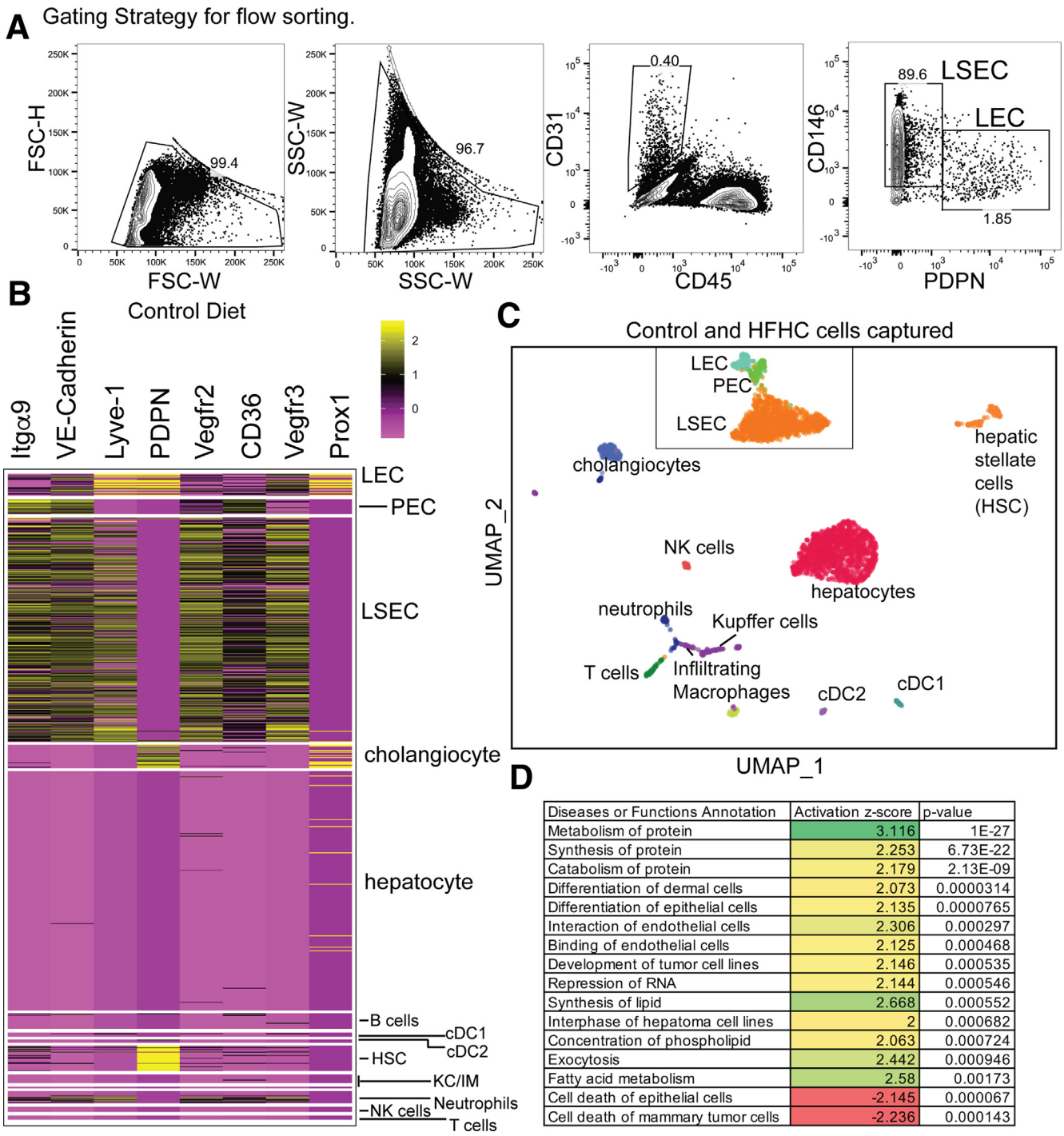

Diseases or Functions Annotation	Activation z-score	p-value
Metabolism of protein	3.116	1E-27
Synthesis of protein	2.253	6.73E-22
Catabolism of protein	2.179	2.13E-09
Differentiation of dermal cells	2.073	0.0000314
Differentiation of epithelial cells	2.135	0.0000765
Interaction of endothelial cells	2.306	0.000297
Binding of endothelial cells	2.125	0.000468
Development of tumor cell lines	2.146	0.000535
Repression of RNA	2.144	0.000546
Synthesis of lipid	2.668	0.000552
Interphase of hepatoma cell lines	2	0.000682
Concentration of phospholipid	2.063	0.000724
Exocytosis	2.442	0.000946
Fatty acid metabolism	2.58	0.00173
Cell death of epithelial cells	-2.145	0.000067
Cell death of mammary tumor cells	-2.236	0.000143

Figure 4. Single-cell sequencing of liver LECs identifies transcriptional changes associated with HFHC diet–induced liver disease. (*A*) Gating strategy used for flow sorting of endothelial cells from control- or HFHC-fed mice. Non-parenchymal cells from the liver were isolated and stained for indicated markers after running through a live/dead selection. All CD31 positive cells were sorted into a single tube and then processed for single-cell RNA sequencing. (*B*) Heatmap of genes typically associated with LECs are shown as a validation of our cell classification. Yellow is genes upregulated and purple is genes downregulated. Shown are cells from control mice. (*C*) Uniform manifold approximation and projection (UMAP) plot to visualize the similarities between cell types acquired using the 10x Genomics single cell sequencing platform. Cells were classified using clustifyr .[55] Inset box shows endothelial cell populations acquired. Shown are cells from control and HFHC mice. (*D*) Gene expression data from LECs only were entered into Ingenuity software for pathway analysis. Shown are pathways with *z*-scores $\geq$2 in LECs from HFHC diet–fed compared with control diet–fed. Green color represents highly activated pathways while red scores represent the downregulation of pathways. Data in figure are combined data from 2–5 mice per capture with 4 independent captures acquired by the 10x Genomics 3′ kit following cell sorting. FSC-H, forward scatter-height; FSC-W, forward scatter-width; HSC, hepatic stellate cell; IM, infiltrating macrophage; KC, Kupffer cell; SSC-W, side scatter-width.

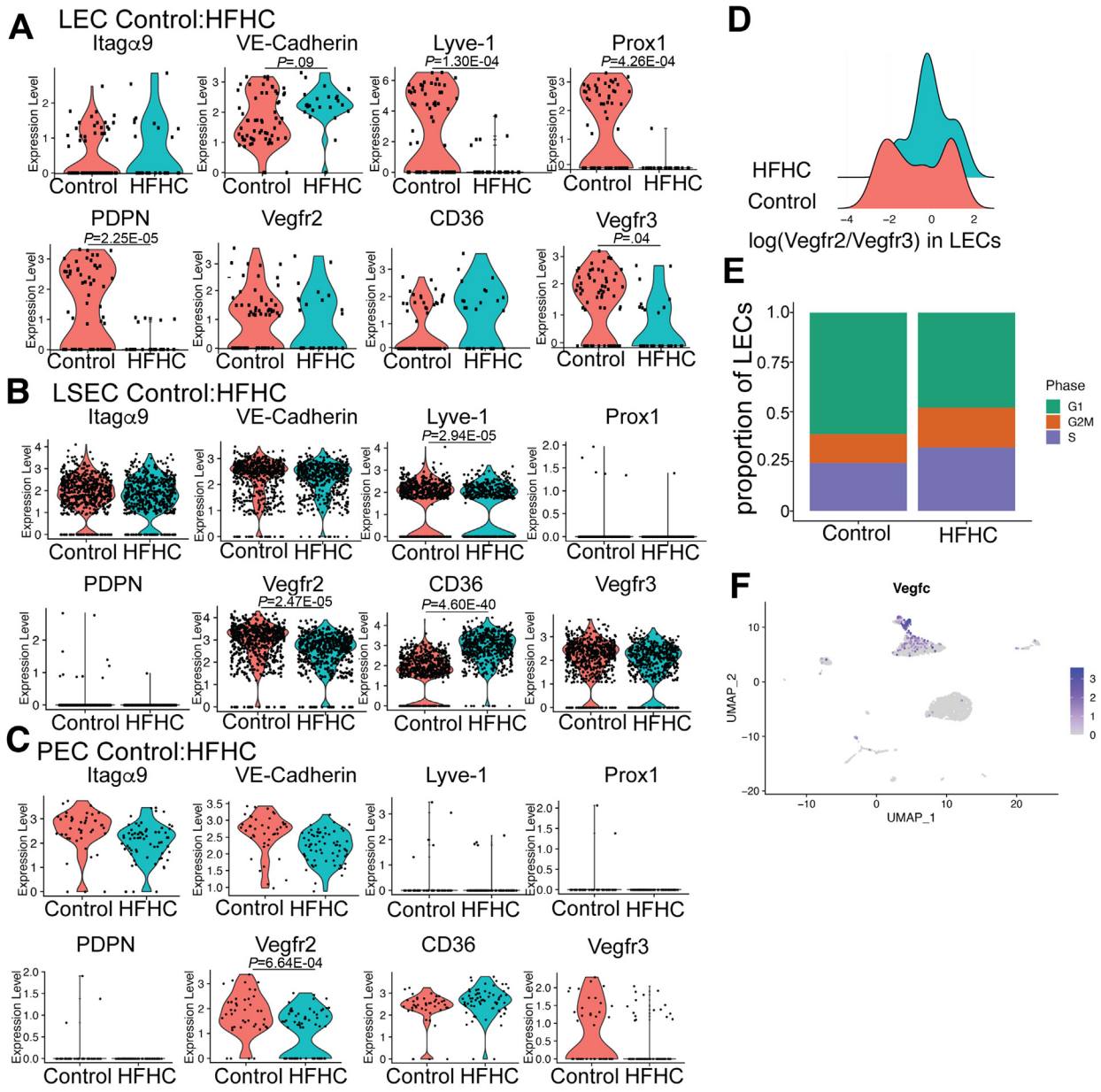

Figure 5. Liver LECs from mice fed an HFHC diet downregulate lymphatic genes and upregulate metabolic pathways. Violin plot of gene expression by (*A*) LECs, (*B*) LSECs, and (*C*) PECs. Shown are changes in gene expression in LECs from the livers of mice fed HFHC diet compared with Control diet. (*D*) Ridge plot showing that the distribution of per-cell *Vegfr2*/*Vegfr3* ratios differs between the LECs from control- and HFHC-fed animals. A cell with a score of 0 in this metric has the average *Vegfr2*/*Vegfr3* ratio, while a cell with a positive score has a higher than average *Vegfr2*/*Vegfr3* ratio. (*E*) Cell cycle analysis of LECs (control/HFHC) based on gene expression from single cell sequencing. (*F*) Uniform manifold approximation and projection (UMAP) representation of *VegfC* expression in single cells where purple indicates increased expression. Cells from control and HFHC livers are shown as in Figure 4*C*. Exact *P* values are shown.

function, required to maintain tissue homeostasis by accommodating for increased fluid and immune infiltrate in the liver, was impacted by disease and could potentially be rescued by rVEGFC. To better understand if diet modulated liver lymphatic function, we utilized a FITC-dextran assay.[42] Specifically, we measured the ability of intrahepatically injected fluorescently labeled dextran to reach to the liver-draining portal LN[43] compared with a non–liver-draining LN (inguinal) (Figure 7*A*). We found that when 500-kD FITC-dextran (the approximate size of LDL that should normally traffic through the lymphatics)[44] was injected into the liver parenchyma of control *C57Bl/6* mice, that the FITC-labeled dextran reached the portal LN within 5 minutes as demonstrated.[42] However, when we examined mice fed the HFHC diet for 20–24 weeks, we found a significant reduction in the amount of FITC-dextran in the portal draining LN

(dLN) compared with the non-draining inguinal LN (Figure 7*B*), suggesting a disruption in lymphatic drainage from the liver of HFHC diet–fed mice that have liver disease (Figure 3*A*–*D*). Importantly, treatment with rVEGFC (cys156ser) restored the drainage to the portal LN while not altering dextran drainage to the inguinal LN (Figure 7*C*) or plasma (Figure 7*D*). Furthermore, we found that this effect was not restricted to 500-kD FITC-dextran as mice fed a

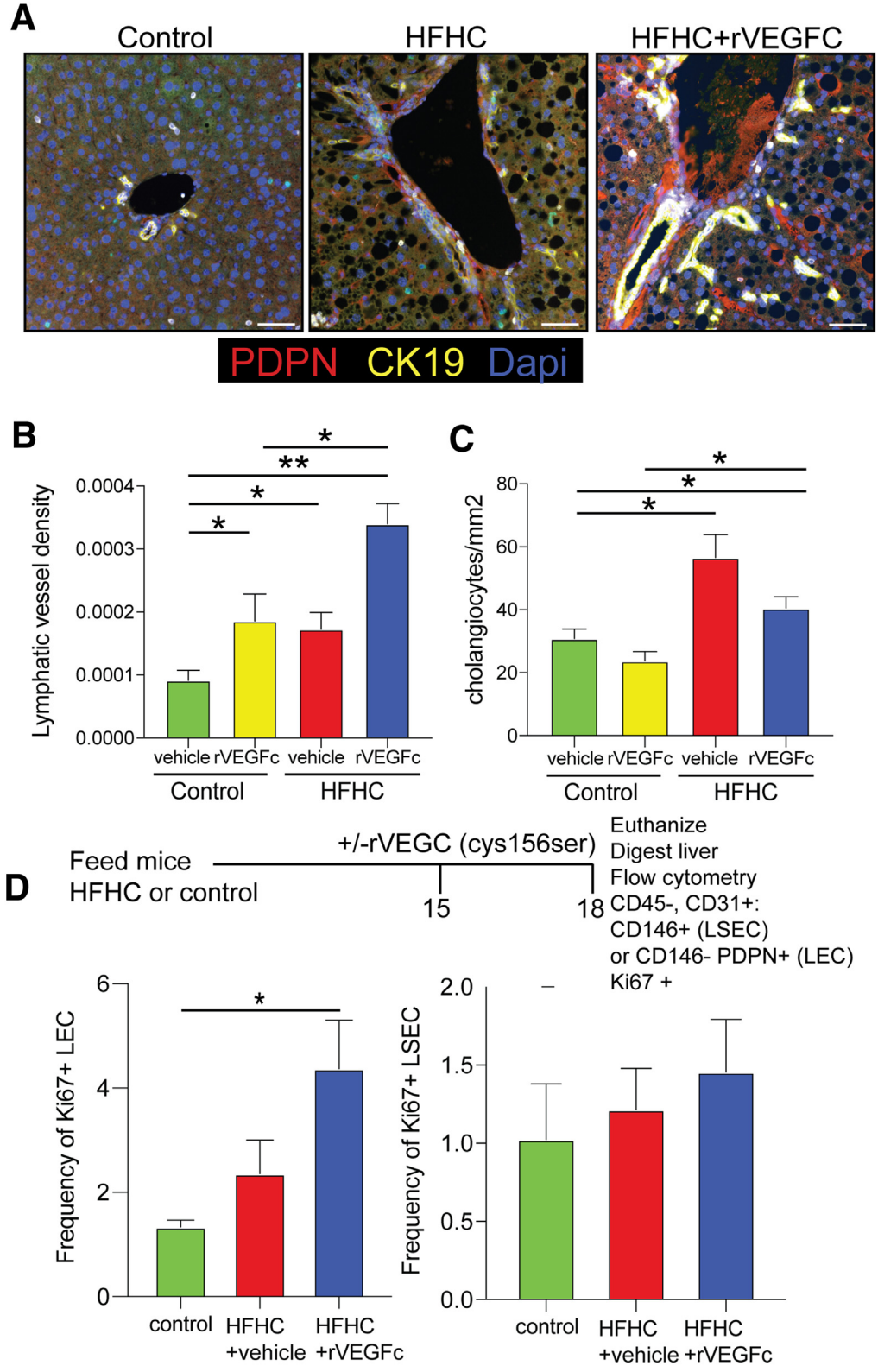

HFHC diet also had less of 70 kD FITC-dextran (the approximate size of albumin) in the portal dLN after intrahepatic injection (Figure 7*E*). We again saw a significant decrease in the expression of PDPN protein by lymphatic vessels in the liver of HFHC-fed mice compared with control-fed mice, by fluorescence intensity; however, the difference was minimized between control and HFHC mice treated with rVEGFC (cys156ser) (Figure 7*F*) suggesting the rVEGFC (cys156ser) not only promoted lymphangiogenesis (Figure 6), but also stabilized lymphatic gene expression. While this rVEGFC (cys156ser) treatment did not result in significant changes in ALT and AST or cholesterol levels, we did observe a moderate decrease in liver inflammation score by histological analysis (Figure 7*G*). This is consistent with an improvement in the ability of the lymphatic vasculature to allow exit of immune cells from the tissue and suggests, consistent with other reports,[36] that rVEGFC treatment improves lymphatic function. Together, these studies demonstrate a significant defect in FITC-dextran transport from the liver to the portal LN of both 70- and 500-kD FITC-dextran during diet-induced liver disease that is rescued by treatment with rVEGFC.

oxLDL Directly Impacts Lymphatic Function in the Liver. Because we have previously published that oxLDL is significantly elevated in the serum[32] of mice fed an HFHC diet and that oxLDL reduces human LEC (hLEC) expression of *PROX1* and *FLT4/VEGFR3* in vitro,[31] we next asked if oxLDL was increased in the liver tissue of mice fed the HFHC diet compared with control mice. We found a significant increase in the amount of oxLDL in the liver of mice fed the HFHC diet compared with age matched control fed mice (Figure 8*A*). As we had noticed similar transcriptional changes in LECs between mice fed the HFHC diet and LECs treated with oxLDL in vitro,[31] we next asked if oxLDL was directly contributing to the changes in lymphatic trafficking of FITC-dextran to the portal dLN. To test this, we administered highly oxidized LDL to mice intravenously over a 2- to 3-week period and then performed the FITC-dextran assay (Figure 8*B*). Strikingly, there was a significant reduction in 500-kD FITC-dextran in the portal dLN, similar to mice fed the HFHC diet, when oxLDL was given intravenously (Figure 8*C*). Moreover, this reduction in FITC-dextran accumulation in the portal dLN following oxLDL administration occurred in the absence of any pathological changes (Figure 8*D*) or inflammatory gene expression in the liver (Figure 8*E*). Furthermore, this difference in FITC-dextran was dependent on the oxidation state of the LDL, as we saw no difference in the amount of FITC-dextran in the portal LN when mice were administered native LDL (Figure 8*F*). These findings demonstrate that oxLDL, even in the absence of inflammation, can directly affect lymphatic function in the liver.

OxLDL Directly Affects Lymphatic Metabolism, Transcription, and Permeability In Vitro. The previous studies in concert with our previously published data demonstrate that oxLDL can have a significant effect on the in vivo function and transcriptional profile of LECs in the liver. As one of the main functions of the lymphatic vasculature is to allow for proteins and cells to pass through the highly permeable button-like junctions,[17] we asked if oxLDL was impacting the permeability of the LECs. First, we confirmed that oxLDL injected in vivo was acquired by LECs using fluorescently labeled oxLDL (Figure 9*A* and *B*).[32] Based on the acquisition of oxLDL by LECs in the liver, we next asked if oxLDL alone was enough to modify LEC function in vitro. It was recently published that LECs, in contrast to vascular endothelial cells, upregulate fatty acid oxidation (FAO) in a positive feedback loop that requires PROX1, p300, and CPT1a to promote lymphatic growth and lymphatic-specific chromatin modifications that differentiate LECs from vascular endothelial cells.[45] As we observed an upregulation of metabolism, catabolism, and protein synthesis in our single-cell pathway analysis, we asked if and how oxLDL changes the metabolic state of LECs. Using mass spectrometry to evaluate metabolites, we discovered an apparent decrease in mitochondrial metabolism in the tricarboxylic acid cycle in LECs following oxLDL treatment (Figure 9*C* and *D*). In the oxLDL-treated LECs, we found a significant reduction in citrate, which is produced from acetyl-CoA via the glycolysis end-product pyruvate, and as a consequence of FAO. Late glycolytic intermediates and pyruvate were not significantly altered by oxLDL treatment, suggesting that the decline observed in citrate and downstream tricarboxylic acid cycle metabolites may be a result of decreased fatty acid metabolism in supplying carbons to the mitochondria (Figure 9*C*–*E*). Combined with our transcriptional data demonstrating a reduction in *Prox1*, *Lyve-1*, *Pdpn*, and *Flt4/Vegfr3* in LECs from mice fed a HFHC diet, after in vitro treatment of LECs with oxLDL,[37] as well as the requirement of *Prox1* to upregulate FAO,[45] these metabolic changes further demonstrate that LECs treated with oxLDL are unable to maintain LEC identity, perhaps making them more like the less permeable vascular endothelial cells, a

Figure 6. (***See previous page***). **VEGFc (cys156ser) regulates lymphangiogenesis but not cholangiocyte or LSEC expansion in the liver.** (*A*) Immunofluorescence staining and quantification of liver sections from indicated groups. Treatment with rVEGFC occurred at 18.5 weeks after initiation of diet and consisted of 2.5 weeks of treatment every other day. Sections were stained with PDPN, CK19, and DAPI. Scale bar is 50 μm. (*B*) Quantification of LVD was performed using inForm software and based on PDPN+CK19– vessels. (*C*) Quantification of cholangiocyte number was performed using ImageJ software and based on PDPN–CK19+ ductal structures. Statistical analysis was performed as in panel *B*. Shown are representative images and combined data from 2 independent experiments with 3–5 mice per group. (*D*) Six-week-old mice were fed a control or HFHC diet for 15 weeks before 3 weeks of rVEGFC or vehicle treatment. At 18 weeks, mice were euthanized and livers were harvested and digested for flow cytometry as in Finlon et al.[54] Indicated markers were used to identify LECs and LSECs and frequency of Ki67+ cells from each type were calculated. Experiment quantified with 4–6 mice per group from 2 independent experiments. Statistical analysis was performed using a Student's *t* test in which $^{*}P < .05$ and $^{**}P < .01$.

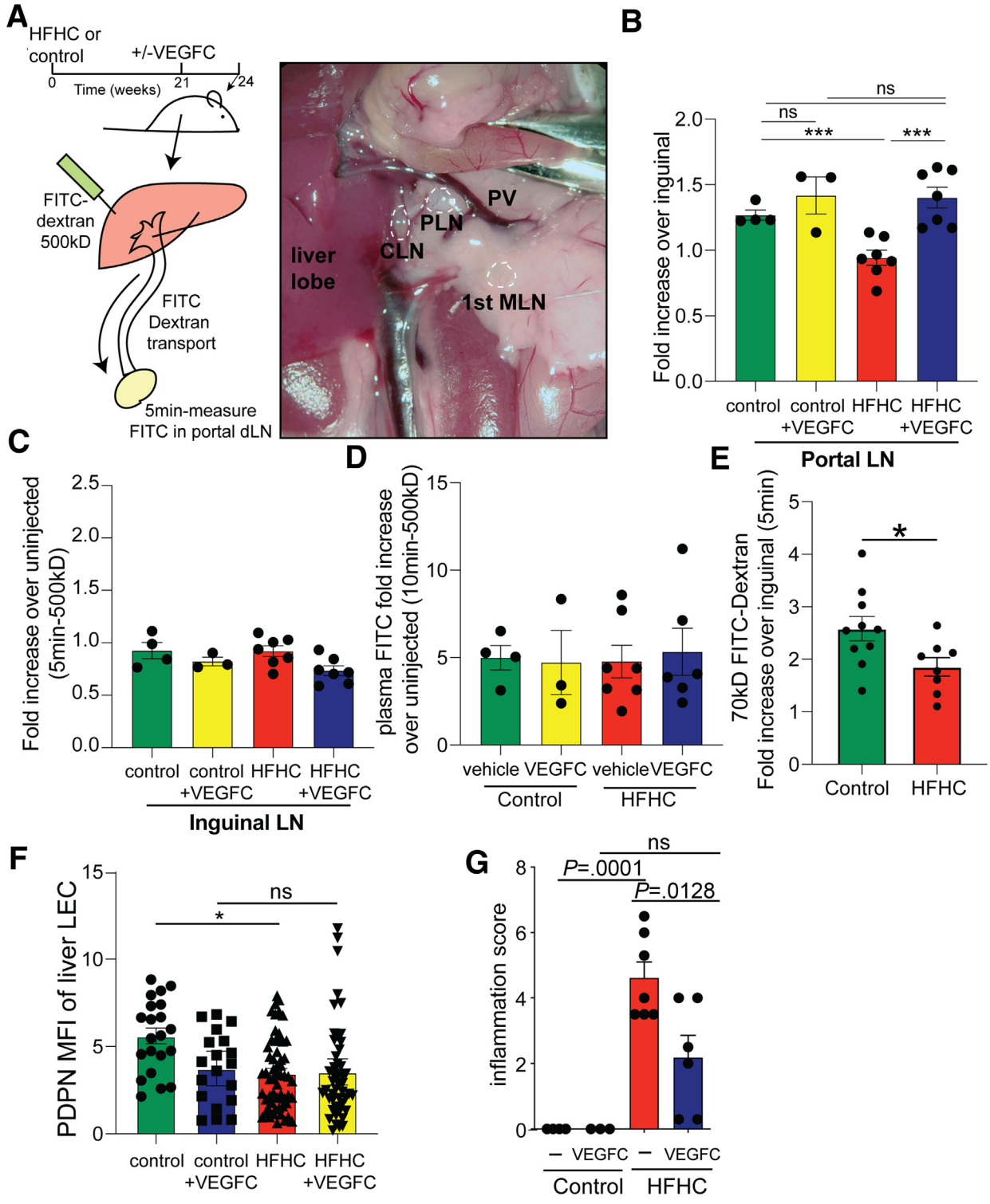

Figure 7. Liver lymphatic transport is impaired in HFHC-fed mice and rescued by rVEGFC. (*A*) Mice were fed with or without administration of rVEGFC (cys156ser). Prior to sacrifice, mice were anesthetized and livers were injected with 5 μL of 500-kD FITC-dextran into each of 3 liver lobes. Five minutes after administration of last injection, the portal-draining LN (PLN) and inguinal lymph nodes were removed. (*B*) Amount of FITC-labeled dextran was measured in portal at 5 minutes. Shown is the fold increase in FITC reading from portal LN to the inguinal lymph node from the same mouse. Fold increase over uninjected in labeled FITC-dextran from (*C*) the inguinal LN or (*D*) plasma. (*E*) Quantification of drainage of 70-kD FITC-dextran to the portal LN at 5 minutes in control or HFHC diet fed mice. (*F*) Mean fluorescence intensity of PDPN protein quantified from analyzed sections using InForm software as in Figure 2*D*. (*G*) Quantification of liver inflammation score by a pathologist blinded to the samples as in Lanaspa et al.[53] Shown are combined data from 2 independent experiments with 3–6 mice per group. Statistical analysis in figure was performed using an unpaired *t* test in which $^{*}P < .05$ and $^{***}P < .001$. CLN, celiac lymph node; dLN, draining lymph node; MLN, mesenteric lymph node; PV, portal vein.

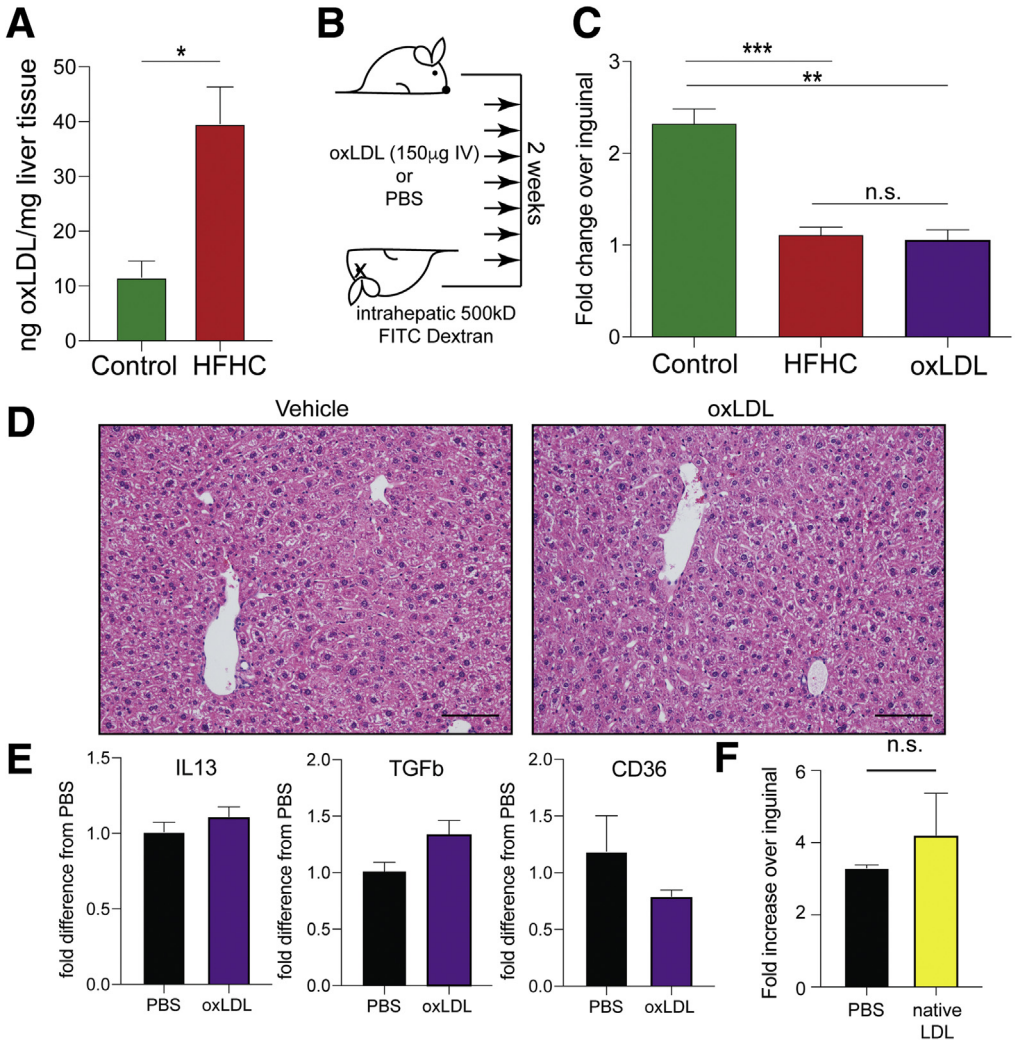

Figure 8. Intravenous injection of oxLDL results in decreased lymphatic drainage. (*A*) Quantification of oxLDL in the liver tissue of mice fed either a control- or HFHC-fed diet for 22 weeks. Shown are combined data from 2 independent experiments with 3–6 mice per group. (*B*) Experimental design for FITC-dextran assay after oxLDL administered intravenously for 2 weeks (every other day for 7 doses). (*C*) As in Figure 7, amount of FITC-dextran in the portal LN of mice injected with PBS given the HFHC diet for 24 weeks or the 7 doses of oxLDL over 2 weeks. Data normalized to nondraining inguinal lymph node from same mouse. (*D*) Representative hematoxylin and eosin images from mice injected with PBS (vehicle) or oxLDL for 2 weeks. No liver injury was observed in any of the mice. Scale bar is 100 μm. (*E*) RT-qPCR for indicated genes from livers of mice given oxLDL systemically. (*F*) 500-kD FITC-dextran drainage assay performed in mice given 150-μg native LDL systemically 7 times over 2 weeks rather than oxLDL as in panel *B*. Shown is representative data from 2 experiments with 3–5 mice per group. OxLDL without HFHC group was performed 1 additional time with 3–6 mice per group with similar results and *P* values. Statistical analysis was performed using an unpaired *t* test in which $^{*}P < .05$, $^{**}P < .01$ and $^{***}P < .001$.

consequence that could directly affect protein and cellular passage into the lymphatic capillaries.

We next asked if these transcriptional and metabolic changes in LECs could lead to differences in the ability of LECs to allow the passage of dextran (in lieu of proteins or cells) through their cell-cell junctions (ie, permeability). To answer this question, we utilized a barrier transwell assay in which a confluent monolayer of hLECs were plated on the upper chamber of a transwell. Using this assay, we found that oxLDL treatment, for either 1 hour or 24 hours, reduced the ability of FITC-dextran to pass through the hLEC monolayer as measured by a decrease in the amount of FITC-dextran found in the lower well (Figure 10*A*). Upon staining with VE-cadherin of hLECs treated with oxLDL, we found a reorganization of the cellular junctions compared with vehicle-treated hLECs. In vehicle-treated hLECs we visualized highly permeable junctions, as demonstrated by distinct VE-cadherin positive junctions between cells. In contrast, oxLDL-treated hLECs had significantly increased staining between cell borders and less distinct junctions (Figure 10*B*). VE-cadherin protein expression by Western blot was significantly increased in hLECs treated with oxLDL (Figure 10*C*), consistent with the increase in fluorescence (Figure 10*B*) and transcription (Figure 5*A*) we found in liver

LECs in mice fed the HFHC diets. We also observed an increase in the ratio of *Vegfr2/Vegfr3* transcript in hLECs treated for 24 hours with oxLDL (Figure 10*D*), consistent with the increased ratio we found in LECs from mice fed the HFHC diet compared with control-fed mice (Figure 5*D*). In contrast, TNFα treatment resulted in increased permeability of the hLECs as previously described (Figure 10*E*).[46] These differences were specific to hLECs, as FITC passage through a layer of human primary umbilical vein endothelial cells (HUVECs) was unchanged following 24-hour treatment of

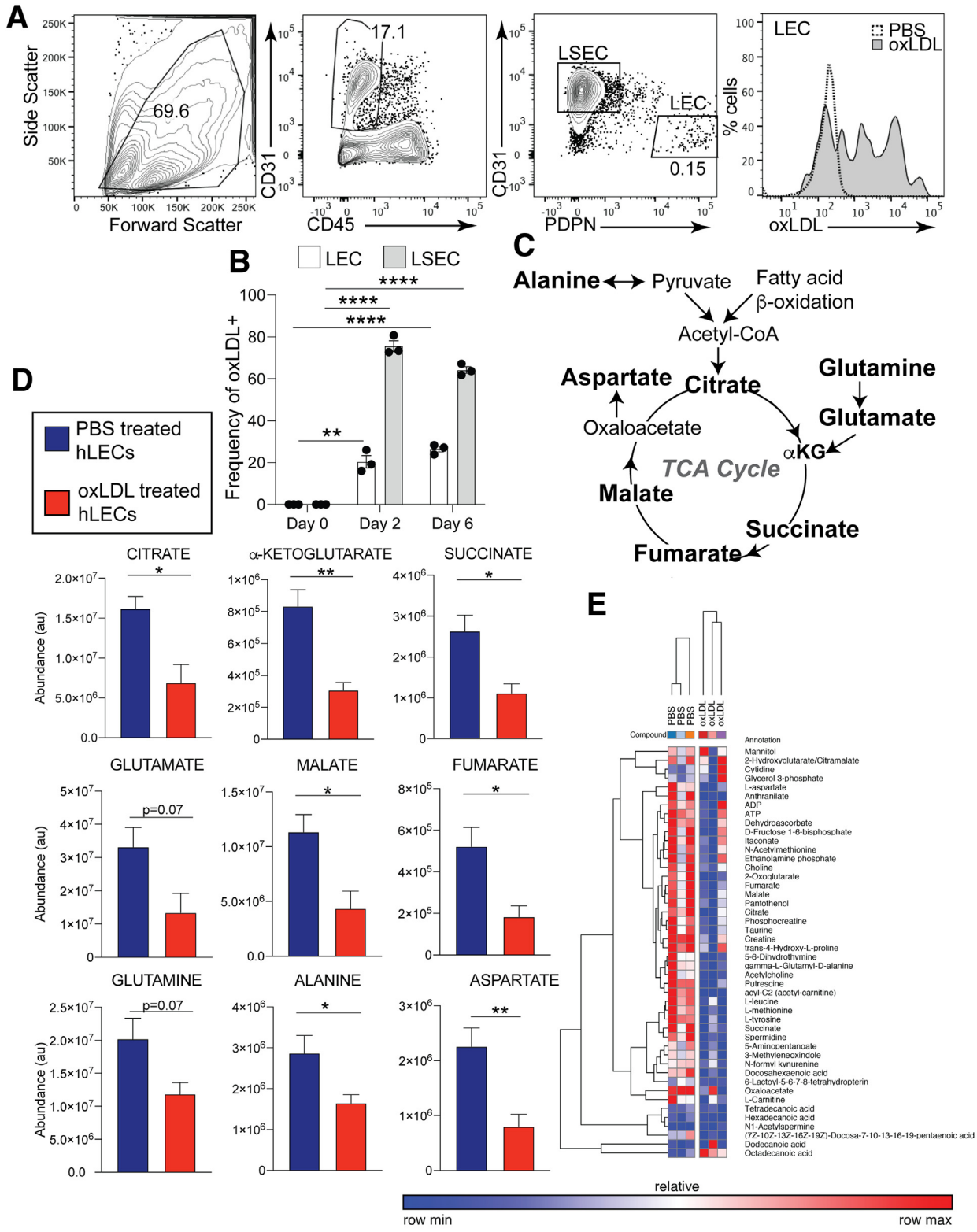

oxLDL (Figure 10*F*), and no changes were observed with HUVECs in either VE-cadherin protein or transcript expression or junctions (Figure 10*G* and *H*). The increased ratio of *Vegfr2/Vegfr3* was also specific to LECs, as we did not observe these changes in HUVECs treated with oxLDL for 24 hours (Figure 10*I*) or LSECs or PECs from mice fed an HFHC diet compared with control (Figure 5*A*–*C*). These findings demonstrate a significant disruption in the ability of hLECs to maintain a lymphatic-specific transcriptional profile,[11] metabolism, and highly permeable button-like junctions in the presence of oxLDL. When combined with our in vivo findings, these studies identify oxLDL as a critical factor that impedes lymphatic function in the liver during NASH and likely contributes to decreased protein homeostasis and inflammatory immune cell removal.

Discussion

Our data, in combination with historical clinical reports and published studies, support a model by which the liver lymphatic system plays a critical role in maintaining protein homeostasis and the exit of inflammatory immune cells from the liver. For decades, it has been appreciated that both the lymphatic vasculature in the liver and the outflow of lymph is dramatically increased in human and animal models of cirrhosis.[7,8] However, it was unknown if these findings were merely a consequence of cirrhosis. The data in this study demonstrate that the liver lymphatic vasculature increases as disease progresses in humans with NAFLD and NASH. These findings are consistent with published observations that chronic liver disease in humans leads to increased expression of prolymphangiogenic growth factors in the liver.[47] Importantly, we find that the LVD in the liver also increases in a well-validated mouse model of NASH; however, our studies demonstrate that even though the lymphatic vasculature expands, the role of the lymphatic vasculature in maintaining protein and immune cell clearance can be compromised by inflammatory mediators like oxLDL. These data increase our confidence that the role of the liver lymphatic vasculature is maintained across species and undergoes dramatic remodeling during the progression of chronic disease.

As noted previously, despite the increased lymphatic vasculature in the liver, and subsequent increased lymph drainage from the liver during cirrhosis, several reports demonstrated that the lymph draining the liver was depleted of high-molecular-weight proteins.[7,48] A major function of the lymphatic vasculature is to allow the transport of proteins and immune cells through permeable button-like junctions, and thus we predicted that the expanded lymphatic vasculature was becoming less permeable during progressive stages of fibrosis and cirrhosis. Using single-cell messenger RNA sequencing we found that several transcripts critical for lymphatic function were decreased in the diseased liver LECs. Specifically, diseased liver LECs had decreased expression of *Prox1*, *Lyve-1*, *Pdpn*, and *Flt4* (Vegfr3). These transcriptional changes are consistent with changes we saw after treatment of LECs with oxLDL.[31] Furthermore, as *Prox1* is required to upregulate FAO,[45] we found that LECs treated with oxLDL had metabolic changes consistent with the decreased FAO and more similar to the metabolic profile of vascular endothelial cells. As *Prox1* also regulates *Vegfr3* expression[11] it is perhaps not surprising that the ratio of *Vegfr2/Vegfr3* is increased. Intriguingly, the balance of expression of the proteins VEGFR2 and VEGFR3, among others, have been shown to regulate the permeability of the lymphatic vasculature.[34] Indeed, hLECs treated with oxLDL have both a significantly different *VEGFR2/VEGFR3* ratio and are significantly less permeable than vehicle-treated LECs. This difference is also consistent in HFHC-fed compared with control-fed mice in which our single-cell analysis demonstrates an increase in the *Vegfr2/Vegfr3* ratio and our in vivo data demonstrate a loss of FITC-dextran accumulation in the portal lymph node.

Together, these findings suggest that liver disease was directly causing a de-differentiation of lymphatic endothelial cells in the liver. Importantly, LECs from diseased liver did not completely adopt a vascular endothelial transcriptional profile. Upon comparison of control LECs to HFHC LECs we found 374 genes were significantly different with a *P* value of $<.01$ (Supplemental Table 1). Interestingly, while 774 genes were differentially regulated between control LECs and control LSECs (a blood endothelial cell) (Supplemental Table 2), 647 genes were differentially regulated between HFHC LECs and HFHC LSECs (Supplemental Table 3). While fewer genes had differential expression between LECs and LSECs from HFHC-fed mice compared with LECs and LSECs from control-fed mice, these cell types are still quite distinct. Thus, our results support the hypothesis that when LECs are exposed to an HFHC diet or oxLDL, they downregulate a

Figure 9. (***See previous page***). **LECs take up oxLDL in vivo and oxLDL treatment in vitro changes LEC metabolism.** (*A*) Gating strategy for liver LEC and LSEC after DIL (1,1'-Dioctadecyl-3,3,3',3-tetramethylindocarbocyanine perchlorate)-labeled oxLDL injection (150 μg intravenously; Kalen Biomedical, Germantown, MD). Shown in the last plot is oxLDL at day 6 in LECs in which the gray histogram is oxLDL injection and white is PBS injection. (*B*) Amount of oxLDL in either LECs (white) or LSECs (gray) at day 2 or day 6 postinjection. Experiment was performed 4 times with similar results. Shown are representative data from 1 experiment that was repeated at least 2 more times with similar results and *P* values. (*C*) Overview of the tricarboxylic acid (TCA) cycle in which bolded metabolites are altered after treatment with oxLDL. (*D*) Changes in bolded metabolites from panel *C*. Metabolite abundance was measured using mass spectrometry in hLECs grown to 80% confluency on a thin layer of matrigel and treated for 24 hours with either vehicle (PBS) (blue) or 100-μg/mL of oxLDL (in PBS) (red) using mass spectrometry. (*E*) Heatmap and hierarchical clustering of changes in metabolites from independent experimental replicates. Experiment was repeated 2 independent times with 3 technical replicates per group. *P* values were calculated using a 1-way analysis of variance with multiple comparisons in which $^{*}P < .05$ and $^{**}P < .01$.

lymphatic gene program that defines at least some of their functions. Ultimately these cells do not become blood endothelial cells, but rather perhaps de-differentiate into an intermediate LEC-Blood endothelial cell phenotype, causing the LECs to perform in a similar manner as their blood progenitors in some respects such as cell-cell junctions and metabolic profile.

Indeed, when we tested if chronic liver disease altered the transport of FITC-dextran from the liver to the portal LN, we found a significant defect, which could be recovered by promoting lymphatic function with rVEGFC. It is important to note that using this assay, the dextran cannot be targeted only to the lymphatic vasculature, and previous studies have demonstrated a loss of LSEC fenestration

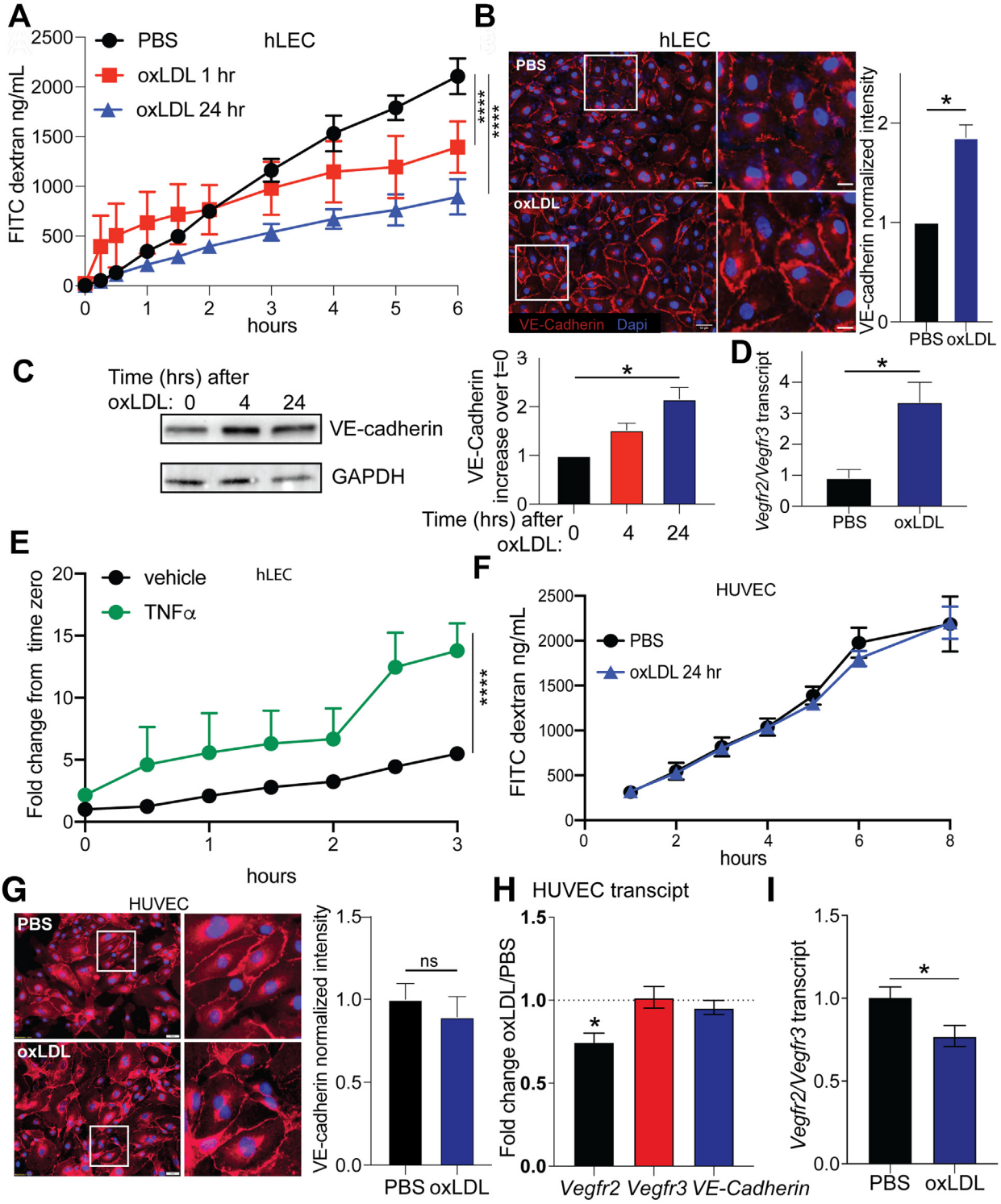

during diet-induced liver disease.[22] As fenestration of LSECs are believed to be key in regulating the protein content of the hepatic lymph, the results reported here are likely detecting changes in the permeability of both sinusoidal and lymphatic endothelium. However, the treatment of mice with the lymphatic growth factor VEGF-C (cys156ser), which did not affect LSEC division and thus may not influence LSEC fenestration, was able to restore lymphatic drainage from the liver of mice fed an HFHC diet. Thus, our studies indicate for the first time a defect in lymphatic function in the liver of mice with chronic liver disease, and that this defect can be rescued with a lymphatic growth factor. Furthermore, we demonstrate that treatment with rVEGFC improves liver inflammation, suggesting a positive link between lymphatic function and liver function.

Our studies focus in on the idea that decreased lymphatic function in the liver, observed during diet-induced disease, is likely a consequence of oxLDL signaling. Our data suggest that oxLDL directly results in a transcriptional and metabolic profile that points to a loss of LEC identity and thus LEC-specific functions. These differences are reflected in the inability of FITC-dextran to properly traffic through the lymphatic endothelial cell junctions, which contributes to the loss of intrahepatically injected FITC-dextran in the portal LN following a 2- to 3-week treatment with intravenous oxLDL. However, understanding how oxLDL affects lymphatic function in the liver, either directly or indirectly, via liver resident cells are the aims of future studies. Indeed, oxLDL was acquired by LECs, LSECs (Figure 9*A* and *B*) and macrophages.[32] As both LSECs and macrophages are likely in close proximity to LECs and could produce other or additional factors which may alter LEC function. While this is a major consideration, the direct impact of oxLDL on LECs that we demonstrate here may provide an opportunity for understanding oxLDL sensing by LECs and the signaling mechanisms involved. Understanding these mechanisms is crucial for the development of effective therapies to improve liver lymphatic function as well as lymphatic function in other organs where the LECs may be exposed to oxLDL in the setting of ongoing disease.

As the rate of liver transplantation continues to rise with a marked increase in end-stage liver disease secondary to NASH, there is an increasing need for the development of therapeutics to slow disease progression. The data in this study highlight the liver lymphatic system as an untapped potential therapeutic target. Similar to published data in the setting of skin,[49] adipose,[50] heart,[51] and kidney[52] inflammation or ischemia-reperfusion injury in the liver,[42] our data demonstrate that administration of recombinant VEGFC can reduce liver inflammation during diet-induced disease. These findings identify the lymphatic system as an attractive target to modulate liver inflammation, maintain protein homeostasis, and slow or reverse the progression of disease in combination with diet modification. Collectively, our data highlight the critical role of the lymphatic system in maintaining liver homeostasis and how disruption of lymphatic function during liver insult acts to potentiate mechanisms of disease.

Materials and Methods

Immunohistochemistry, Microscopy, and Liver Histology

For Human studies, liver biopsies were obtained from the University of Colorado Anschutz Research Histology Shared Resource. For patient demographics see table 1. Biopsies were cut in 5-μm-thick sections and adhered to a glass slide. Slides were deparaffinized and antigen retrieval

Figure 10. (*See previous page*). OxLDL treatment changes LEC permeability and VE-cadherin expression. (*A*) A total of 6–10,000 hLECs were plated onto a transwell with 0.4-μm pores and allowed to form a basement membrane for 3 days. After 3 days, the hLECs were treated with oxLDL for 1 hour or 24 hours prior to the addition of 500-kD FITC-Dextran to the top well. Hanks' balanced salt solution in the bottom well was removed at indicated time points and the amount of FITC-dextran in the bottom well was measured. Linear regression was performed and determined that the slope of the line was significantly different with a *P* value of $<.0001$ as indicated by 4 stars. Data shown are from 1 independent experiment with at least 3 replicates per group. Experiment was repeated at least 2 additional times with similar results and *P* values. (*B*) Transwell inserts were removed from the plate and stained with VE-cadherin (red) and DAPI (blue). Shown are junctions between cells in which the scale bar on the larger images is 50 μm and the white box is zoomed in and on the right. Scale bar on zoomed out image is 10 μm. Quantification of VE-cadherin pixel intensity from 3 replicates normalized to the PBS control is shown. (*C*) Protein expression of VE-cadherin was calculated from cells treated with oxLDL as in panel *B* for either 4 or 24 hours. Shown is Western blot analysis using antibodies against VE-cadherin and GAPDH (loading control). Western blot was performed 3 times and quantification is shown from replicates normalized to time 0. (*D*) *Vegfr2*/*Vegfr3* transcript ratio assessed by RT-qPCR of hLECs treated with 100 μg oxLDL or PBS for 24 hours. Experiment was repeated 3 times with similar results. (*E*) A total of 6–10,000 hLECs were seeded on a transwell as in panel *A* and treated with 1-ng TNFα (10 ng/mL) in 100-μL PBS (vehicle) and the amount of FITC-dextran recovered from the bottom well was measured every 30 minutes over a 3-hour period. Shown is fold change from time 0 before FITC was added to the top well. Shown are data from 1 experiment with 3 technical replicates. Experiment was repeated at least twice with similar results. Linear regression was performed and determined that the slope of the line was significantly different with a *P* value of $<.0001$ as indicated by 4 stars. (*F*) As in panel *A*, 0.4-μm transwell plated with a confluent layer ($\sim$10,000 cells for 2–3 days) of HUVECs. Cells were treated with either PBS (black) or oxLDL (100 μg) (blue) for 24 hours prior to the addition of 500-kD FITC-dextran. At indicated timepoints, FITC-dextran was recovered from the bottom well and read on a fluorescent plate reader. Differences were not significant. (*G*) Cells from panel *F* were stained with VE-cadherin and fluorescence intensity was calculated as described previously. (*H*) Cells treated as in panels *F* and *G* were removed from the plate and RNA was isolated for quantification of relative levels of transcript based on amount of complementary DNA made. Fold increase over PBS is shown for indicated genes. (*I*) Ratio of *Vegfr2*/*Vegfr3* transcript in HUVECs following treatment with either PBS or oxLDL. Experiment was repeated at least twice with similar results. $^*P < .05$.

was done in TRS (Dako, Carpinteria, CA). Slides were blocked for 5 minutes in 0.3% hydrogen peroxide, followed by an hour block in 2% bovine serum albumin (BSA). Mouse anti-human PDPN (1:50, clone D2-40; Dako) was added to the biopsies for 2 hours. Anti-mouse secondary conjugated to HRP (Dako) was added for 30 minutes. DAB+ was used as the visualizing agent, and the slides were counterstained with hematoxylin. Whole slide images were taken using an Olympus IX83 microscope with a ZDC laser-based focusing system (Olympus, Tokyo, Japan). For analysis of lymphatic vessels in murine livers, at the time of harvest the median lobe of the liver was excised, the gallbladder was removed and tissue was fixed in 10% neutral buffered formalin at room temperature for 24 hours. Livers were then embedded in paraffin, cut into 5-μm-thick sections, placed on a glass slide, and stained as described.[31] Briefly, slides were dewaxed with xylene, heat-treated in either pH 6 or pH 9 antigen retrieval buffer for 15 minutes in a pressure cooker, and blocked in antibody diluent (PerkinElmer, Waltham, MA). Sections were then sequentially stained for PDPN (8.1.1), Lyve-1 (ab33682), and CK19 (ab52625) primary antibodies followed by HRP-conjugated secondary polymer (anti-rabbit [PerkinElmer], anti-goat ab97110, or anti-hamster ab6892) and HRP-reactive OPAL fluorescent reagents (PerkinElmer). To image nuclei, slides were stained with spectral DAPI and coverslips were applied with Prolong Dimond mounting media (Thermo Fisher Scientific, Waltham, MA). Data were collected using the Vectra 3.0 Automated Quantitative Pathology Imaging system (PerkinElmer) as described.[31] For quantification of PDPN and Lyve-1 fluorescence intensity, lymphatic vessels were identified, the lumen of the vessel was subtracted from analysis, and the median intensity of PDPN or Lyve1 in the vessel area was calculated with inForm software (PerkinElmer). For Ki67 staining, anti-mouse Ki67 (clone SP6; Thermo Fisher Scientific), staining was performed with the previously mentioned antibodies to determine Ki67+ lymphatic vessels. Number of Ki67+ lymphatic vessels were manually counted from entire section and value per millimeter squared was determined. This study was approved by the institutional review board at the University of Colorado Anschutz Medical Campus.

Animal Studies and Feeding Regimens

All experiments utilized 6- to 8-week-old male C57BL/6 mice purchased from Charles River Laboratories (Wilmington, MA). For diet studies, mice were randomly allocated to either a chow control or HFHC diet (#D17010101-03) formulated by Research Diets Inc. (New Brunswick, NJ) and as described in McGettigan et al.[32] Mice were provided diet ad libitum for a period between 20 and 32 weeks. For treatment studies, mice were injected (intraperitoneally) with rVEGFC (cys156ser) (10 mg/kg per dose) or every 2 days for 3 weeks. For studies of oxLDL regulation of lymphatic permeability, mice were injected intravenously with 150 μg of highly oxidized LDL (Kalen Biochemicals, Germantown, MD) or phosphate-buffered saline (PBS) as a vehicle control in a total volume of 200 μL. Injections of oxLDL or vehicle occurred twice weekly for a period of 1–2 weeks. All animal studies were approved by the University of Colorado Anschutz Institutional Animal Care and Use Committee.

Quantification of Liver Pathology

For quantification of liver histology, liver sections were stained with hematoxylin and eosin and scored semi-quantitatively for steatosis and inflammation as previously described.[53] Briefly, liver sections were given a numeric score for each feature within a given pathology category. Within each category individual pathological features were given a numerical score (0–4) based on how prevalent it was. Thus, the total scores for each pathology category (steatosis (max score 5) and inflammation (max score 14) were simply a sum of the individual scores for each feature. Histology scoring of blinded liver sections was performed by D.J.O., who was blinded to the identity of the liver section being scored.

Quantification of Serum and Liver Cholesterol Levels and Liver Enzymes

Age- and sex-matched mice were fed either a control chow or HFHC diet, and plasma was obtained during the course of feeding via submandibular bleed or at the time of harvest with cardiac puncture. Whole blood was allowed to clot at room temperature for 10 minutes and serum was isolated by centrifugation. For analysis of liver cholesterol, portions of livers were weighed and subjected to analysis. Determination of cholesterol levels was performed using the cholesterol assay kit (ab65390; Abcam, Cambridge, United Kingdom) exactly as described by the manufacturer. Measurement of serum AST and ALT (lower limit 10 U/l; Fuji Dri-Chem Slide GPT/AST) obtained using a DriChem 7000 Veterinary Chemistry Analyzer (Heska, Loveland, CO).

Quantification of Liver oxLDL

Liver tissue was obtained at the time of harvest, weighed, rinsed with PBS to remove excess blood and homogenized with a glass homogonizer. OxLDL levels were determined using a mouse oxLDL ELISA kit (MBS2512757; Mybiosource, San Diego, CA) per manufacturer instructions.

Semi-Quantitative PCR

Briefly, snap-frozen liver tissue or cultured cells were homogenized in Buffer RLT and total RNA was isolated from cell lysate using the RNeasy Mini Kit (Qiagen, Hilden, Germany), and complementary DNA was synthesized using the QuantiTect RT Kit (Qiagen) following standard protocols. PCR amplification was performed using either the QuantiTect Syber green (Qiagen) or TaqMan Fast Advanced Master Mix (Applied Biosystems, Foster City, CA) PCR kits. Quantitative PCR was performed on a QuantStudio 3 Real-time PCR machine (Applied Biosystems) and fold changes in messenger RNA levels were calculated. For each gene, all samples were normalized to the average fold change of the control treatment group (chow or PBS). The following

Qiagen QuantiTect primer assays were used: 18S ribosomal RNA (Rn18s; QT02448075), transforming growth factor beta 1 (Tgfb1; QT00145250), CD36 (QT01058253), and IL13 (QT00099554) for mouse and VEGFC FWD: 5′ ccacgtgaggtgtgtatagatg 3′, VEGFC REV: 5′ ctgcctgacactgtggtaat 3′; for human: VEGFR2(KDR): QT00069818, VEGFR3(FLT4):QT000063637, VE-Cad (CDH5): QT000013244 and GusB (housekeeping gene): QT000046046.

Quantification of LVD

LVD is defined as the area of the lymphatics divided by the area of the defined tissue area. For lymphatic density in human biopsies, images were opened in photoshop. Approximately nine 600 × 500 pixel areas were used and portal triads were cut out of the image. Each area (75 mm^2) contained 6–9 portal triads that were evaluated per biopsy in which the lymphatic vessel was masked, area calculated, and then divided by the total area. Lymphatics were colored in using the color tool and the whole 1800 × 1500 area was opened with ImageJ version 1.52T (National Institutes of Health, Bethesda, MD). The image was converted into an 8-bit image and the threshold was adjusted so only the drawn lymphatic area was seen. The analyze particles function was used to determine the area of the lymphatics. Area of lymphatics was then divided by the total area of cut out image. For analysis of murine livers, LVD was quantified with Nikon AR software version 4.60 (Nikon, Melville, NY) as described.[31] Regions of approximately 1.3 mm^2 were randomly selected and the area of the lymphatic vessel was determined in the entire area, in which at least 2 portal triads were in the field of measurement. LVD was calculated as the area of the vessels divided by the area of the tissue.

Liver Cell Isolation and Fluorescence-Activated Cell Sorting

Briefly, murine livers were harvested and non-parenchymal cells were isolated as previously described.[54] Following isolation, cells were washed 2× with PBS and dead cells were removed using the EasySep Dead Cell Removal Kit (Stem Cell Technologies, Vancouver, Canada). Viable cells were washed 2× with PBS containing 0.5% fetal bovine serum (Atlas Biologicals, Fort Collins, CO) and stained with antibodies against CD45 (30-F11), CD31 (390), CD146 (ME-9F1), and PDPN (8.1.1) from BioLegend (San Diego, CA). Cells were washed twice and were sorted using an aria Fusion sorter (BD Biosciences, Franklin Lakes, NJ). Enriched stromal cells were then washed 2× with PBS and subjected to single cell sequencing as described subsequently.

Single-Cell RNA Sequencing

Approximately 10,000 viable enriched stromal cells were loaded on a 10x Genomics controller (10x Genomics, San Francisco, CA) to generate barcoded single-cell Gel Bead in-Emulsions (GEMs) using the 10x Genomics 3′ kit as previously described.[31] Complementary DNA libraries were sequenced using a NovaSeq 6000 (Illumina, San Diego, CA) at the University of Colorado Genomics Shared Resource Core. To control for batch effects 3 independent sequencing experiments were performed which included both control- and HFHC diet–fed mice. Quantification and analysis of single cell sequencing was performed using the R packages Seurat and scran as previously described.[31] Ridge plots were generated using Seurat's RidgePlot function. Cells were classified and correlation plots were generated using clustifyr.[55] For cell cycle analysis, Seurat assigns each cell a score based on its expression of G2/M and S phase markers. These marker sets are anti-correlated in their expression levels, and cells expressing neither are assigned to G1 phase. Cells with fewer than 250 detectable genes or >20% of unique molecular identifiers (UMIs) derived from mitochondrial genes were excluded from the analysis to eliminate cells with insufficient expression data for clustering and dead cells, respectively.

Liver Lymphatic Drainage Assay

Control or HFHC diet–fed mice or mice injected with oxLDL (150 μg) or PBS were anesthetized with 2%–2.5% isoflurane or a solution of ketamine (30–60 mg/kg) and xylazine (3–6 mg/kg) and placed on a heating pad. An incision was made into the peritoneum to expose the liver and 5 μL of a solution of 10 mg/mL of FITC-labeled dextran (70 or 500 kD) in PBS was injected into left, median, and right lobes of the liver using a 28-gauge needle (BD Biosciences). Five minutes after FITC-dextran administration, the liver-draining LN (portal) were excised and placed into separate wells containing 400-μL PBS. As a control for vascular drainage of the dextran, the inguinal (skin draining) LN was also excised. LNs were minced with 22-gauge needles, and 200 μL of the minced LN in PBS was placed in a 96-well Costar Assay Plate (Corning, Corning, NY), and FITC was read using a Synergy H1 microplate fluorescence plate reader (BioTek, Winooski, VT). Data were normalized to the inguinal LN from the same mouse taken immediately after the portal LN.

In Vitro Permeability Assay

Briefly, 6000–10,000 human lymphatic endothelial cells (hLECs) (PromoCell, Heidelberg, Germany) or HUVECs were plated on a 0.2% gelatin–coated 24-well Costar Transwell permeable support (6.55-mm insert) with a 0.4 mm Polyster Membrane (Corning). hLECs on the transwell were then stained for VE-Cadherin by either immunofluorescence or Western blot. A total of 72 hours following plating, cells were incubated with oxLDL (100 μg/mL), TNFα (10 ng/mL), or vehicle control (PBS) for 1 hour or 24 hours. Following incubation, 500-kD FITC Dextran (100 μg/mL) in Hanks' balanced salt solution was added to the top of the well. Media were removed from the bottom of the transwell and replaced with HBSS. Plates were incubated at 37°C with gentle rocking and migration of the FITC-labeled dextrans was measured using a Synergy H1 microplate reader by removing 60 μL from the bottom of the transwell at indicated time points at an excitation of 485 nm and emission of 528 nm. For quantification of

FITC, a standard curve of FITC-dextran was read along with experimental samples. The actual amount of FITC-dextran was then calculated using the equation of the line based on the standard curve generated on the same day.

VE-Cadherin Staining

Human dermal lymphatic endothelial cells (hdLEC) staining of cells from in vitro permeability assay in the 24-well transwell plate were fixed after assay was complete with 4% paraformaldehyde for 15 minutes at room temperature. Cells were then rinsed and blocked with 10% donkey serum, 2% BSA, for 1 hour at room temperature. Staining was performed with rabbit anti-VE-cadherin 1:100 (Abcam) and DAPI 1:1000 (BioLegend). The filter was removed from the transwell insert and mounted on a microscope slide and read on an Olympus microscope using cellSens 1.16 software. Quantification of pixel intensity was performed using photoshop (Adobe, San Jose, CA). Fluorescence from VE-cadherin was measured in the red color channel, and then 3 equally sized areas from each experiment were measured by mean gray value using the measurement log function for both the PBS- and oxLDL-treated samples. The 3 measurements from each sample were averaged and divided by the PBS value average to obtain fold increase over PBS ($*P < .05$).

Western Blots

hLECs were grown to >80% confluency in T25 flasks then treated with oxLDL at 100 mg/mL for either 4 or 24 hours. Treated as well as untreated cells were washed twice with cold PBS and cells were coated with 500 μL of lysis buffer (from RayBiotech kit AAH-MAPK-1-2 prepared with supplied protease and phosphatase inhibitors to manufacturer instructions). Flasks were then immediately moved to −80°C and froze overnight. Cells were thawed and scraped into the lysis buffer. Lysate was collected and clarified by spinning at >12,000 g for 20 minutes. Supernatant was collected and quantified using BCA kit (23225; Thermo Fisher Scientific). Gel samples were made by combining equal amounts of protein from each sample diluted to equal volume with lysis buffer. 4× Laemmli buffer with 10% 2-mercaptoethanol was added for a final concentration of 1×, then samples were heated on a heat block of 90°C for 10 minutes. Samples were run on 10% acrylamide gels and transferred to 0.45-μm polyvinylidene difluoride membrane. Membranes were blocked with 5% BSA/Tris-buffered saline with 0.1% Tween 20 detergent [TBST] for 30–60 minutes at room temperature while rocking. Then membranes were incubated in anti-VE-cadherin (AB33168 [Abcam] dilulted 1:1000 or 1 μg/mL in 3% BSA/TBST) or anti-GAPDH-HRP (MA5-15738-HRP; Invitrogen, Carlsbad, CA) overnight at 4°C while rocking. Membranes were then washed with TBST 3 × 5 minutes then for VE-Cadherin incubated with anti-Rabbit-HRP (AB7090 [Abcam] 1:10,000 in 3% BSA/TBST) at room temperature for 1 hour while rocking. Membranes were then washed 3 × 5 minutes in TBST and imaged using Pierce ECL western blotting substrate and the ChemiDoc MP imaging system (Bio-Rad, Hercules, CA). Quantification of Western blot was performed using ImageLab (Bio-Rad) analysis software. Pixel intensity was quantified for each band and then normalized to the loading control for each individual sample before dividing the values by the time zero values in order to obtain the fold increase over time zero.

Metabolite Analysis

Mass spectrometry-based metabolomics was performed on frozen cell pellets. Cells were extracted at 2×10^6 cells per mL in ice-cold lysis/extraction buffer (methanol:acetonitrile:water 5:3:2) and analyzed using a 5-minute C18 gradient on a Vanquish UHPLC system coupled online to a Q Exactive mass spectrometer (Thermo Fisher Scientific). Sample preparation, data acquisition, and data analysis were performed exactly as described.[56]

Statistical Analysis

All statistical analysis was performed using a Student's t test or 1-way analysis of variance with multiple comparisons to obtain a P value. P values are designated by asterisks in which $*P < .05$, $**P < .01$, $***P < .001$, $****P < .0001$. The number of animals used per experiment was determined based on a power calculation.[57,58] Statistically significant differences between control and experimental groups ($P \leq .05$ with determined number of animals per group based on power calculation) were obtained in 2 experiments (1+1 repeat). If in 1 of the 2 experiments the significance level did not attain at least $P \leq .05$, a third and deciding repeat was performed. Based on our Institutional Animal Care and Use Committee (IACUC) protocol, unnecessary animal experiments were not performed. For in vitro experiments, all experiments were performed a minimum of 3 independent times with 3–5 replicates per group. All authors had access to the study data and had reviewed and approved the final manuscript.

References

1. Habka D, Mann D, Landes R, Soto-Gutierrez A. Future economics of liver transplantation: a 20-year cost modeling forecast and the prospect of bioengineering autologous liver grafts. PLoS One 2015;10:e0131764.
2. Noureddin M, Vipani A, Bresee C, Todo T, Kim IK, Alkhouri N, Setiawan VW, Tran T, Ayoub WS, Lu SC, Klein AS, Sundaram V, Nissen NN. NASH leading cause of liver transplant in women: updated analysis of indications for liver transplant and ethnic and gender variances. Am J Gastroenterol 2018;113:1649–1659.
3. Randolph GJ, Ivanov S, Zinselmeyer BH, Scallan JP. The lymphatic system: integral roles in immunity. Annu Rev Immunol 2017;35:31–52.
4. Lim HY, Thiam CH, Yeo KP, Bisoendial R, Hii CS, McGrath KC, Tan KW, Heather A, Alexander JS, Angeli V. Lymphatic vessels are essential for the removal of cholesterol from peripheral tissues by SR-BI-mediated transport of HDL. Cell Metab 2013;17:671–684.

5. Platt AM, Rutkowski JM, Martel C, Kuan EL, Ivanov S, Swartz MA, Randolph GJ. Normal dendritic cell mobilization to lymph nodes under conditions of severe lymphatic hypoplasia. J Immunol 2013;190:4608–4620.
6. Barrowman JA, Granger DN. Effects of experimental cirrhosis on splanchnic microvascular fluid and solute exchange in the rat. Gastroenterology 1984;87:165–172.
7. Dumont AE, Mulholland JH. Flow rate and composition of thoracic-duct lymph in patients with cirrhosis. N Engl J Med 1960;263:471–474.
8. Dumont AE, Mulholland JH. Alterations in thoracic duct lymph flow in hepatic cirrhosis: significance in portal hypertension. Ann Surg 1962;156:668–675.
9. Petrova TV, Makinen T, Makela TP, Saarela J, Virtanen I, Ferrell RE, Finegold DN, Kerjaschki D, Yla-Herttuala S, Alitalo K. Lymphatic endothelial reprogramming of vascular endothelial cells by the Prox-1 homeobox transcription factor. EMBO J 2002:214593–214599.
10. Wigle JT, Oliver G. Prox1 function is required for the development of the murine lymphatic system. Cell 1999; 98:769–778.
11. Johnson NC, Dillard ME, Baluk P, McDonald DM, Harvey NL, Frase SL, Oliver G. Lymphatic endothelial cell identity is reversible and its maintenance requires Prox1 activity. Genes Dev 2008:223282–223291.
12. Rauniyar K, Jha SK, Jeltsch M. Biology of vascular endothelial growth factor C in the morphogenesis of lymphatic vessels. Front Bioeng Biotechnol 2018;6:7.
13. Wilting J, Papoutsi M, Christ B, Nicolaides KH, von Kaisenberg CS, Borges J, Stark GB, Alitalo K, Tomarev SI, Niemeyer C, Rossler J. The transcription factor Prox1 is a marker for lymphatic endothelial cells in normal and diseased human tissues. FASEB J 2002; 16:1271–1273.
14. Nelson GM, Padera TP, Garkavtsev I, Shioda T, Jain RK. Differential gene expression of primary cultured lymphatic and blood vascular endothelial cells. Neoplasia 2007;9:1038–1045.
15. Amatschek S, Kriehuber E, Bauer W, Reininger B, Meraner P, Wolpl A, Schweifer N, Haslinger C, Stingl G, Maurer D. Blood and lymphatic endothelial cell-specific differentiation programs are stringently controlled by the tissue environment. Blood 2007; 109:4777–4785.
16. Nitti MD, Hespe GE, Kataru RP, Garcia Nores GD, Savetsky IL, Torrisi JS, Gardenier JC, Dannenberg AJ, Mehrara BJ. Obesity-induced lymphatic dysfunction is reversible with weight loss. J Physiol 2016; 594:7073–7087.
17. Baluk P, Fuxe J, Hashizume H, Romano T, Lashnits E, Butz S, Vestweber D, Corada M, Molendini C, Dejana E, McDonald DM. Functionally specialized junctions between endothelial cells of lymphatic vessels. J Exp Med 2007;204:2349–2362.
18. Jackson DG. Leucocyte trafficking via the lymphatic vasculature- mechanisms and consequences. Front Immunol 2019;10:471.
19. Gao S, Liu J. Association between circulating oxidized low-density lipoprotein and atherosclerotic cardiovascular disease. Chronic Dis Transl Med 2017;3:89–94.
20. Ho CM, Ho SL, Jeng YM, Lai YS, Chen YH, Lu SC, Chen HL, Chang PY, Hu RH, Lee PH. Accumulation of free cholesterol and oxidized low-density lipoprotein is associated with portal inflammation and fibrosis in nonalcoholic fatty liver disease. J Inflamm (Lond) 2019; 16:7.
21. Yimin, Furumaki H, Matsuoka S, Sakurai T, Kohanawa M, Zhao S, Kuge Y, Tamaki N, Chiba H. A novel murine model for non-alcoholic steatohepatitis developed by combination of a high-fat diet and oxidized low-density lipoprotein. Lab Invest 2012;92:265–281.
22. Zhang Q, Liu J, Liu J, Huang W, Tian L, Quan J, Wang Y, Niu R. oxLDL induces injury and defenestration of human liver sinusoidal endothelial cells via LOX1. J Mol Endocrinol 2014;53:281–293.
23. Ampuero J, Ranchal I, Gallego-Duran R, Pareja MJ, Del Campo JA, Pastor-Ramirez H, Rico MC, Picon R, Pastor L, Garcia-Monzon C, Andrade R, Romero-Gomez M. Oxidized low-density lipoprotein antibodies/high-density lipoprotein cholesterol ratio is linked to advanced non-alcoholic fatty liver disease lean patients. J Gastroenterol Hepatol 2016;31:1611–1618.
24. Nakhjavani M, Mashayekh A, Khalilzadeh O, Asgarani F, Morteza A, Omidi M, Froutan H. Oxidized low-density lipoprotein is associated with viral load and disease activity in patients with chronic hepatitis C. Clin Res Hepatol Gastroenterol 2011;35:111–116.
25. Schroder H, Marrugat J, Fito M, Weinbrenner T, Covas MI. Alcohol consumption is directly associated with circulating oxidized low-density lipoprotein. Free Radic Biol Med 2006;40:1474–1481.
26. Karadeniz G, Acikgoz S, Tekin IO, Tascylar O, Gun BD, Comert M. Oxidized low-density-lipoprotein accumulation is associated with liver fibrosis in experimental cholestasis. Clinics (Sao Paulo) 2008;63:531–540.
27. Bieghs V, van Gorp PJ, Walenbergh SM, Gijbels MJ, Verheyen F, Buurman WA, Briles DE, Hofker MH, Binder CJ, Shiri-Sverdlov R. Specific immunization strategies against oxidized low-density lipoprotein: a novel way to reduce nonalcoholic steatohepatitis in mice. Hepatology 2012;56:894–903.
28. Ekstedt M, Franzen LE, Mathiesen UL, Holmqvist M, Bodemar G, Kechagias S. Statins in non-alcoholic fatty liver disease and chronically elevated liver enzymes: a histopathological follow-up study. J Hepatol 2007; 47:135–141.
29. Schierwagen R, Maybuchen L, Hittatiya K, Klein S, Uschner FE, Braga TT, Franklin BS, Nickenig G, Strassburg CP, Plat J, Sauerbruch T, Latz E, Lutjohann D, Zimmer S, Trebicka J. Statins improve NASH via inhibition of RhoA and Ras. Am J Physiol Gastrointest Liver Physiol 2016; 311:G724–G733.
30. Eslami L, Merat S, Malekzadeh R, Nasseri-Moghaddam S, Aramin H. Statins for non-alcoholic fatty liver disease and non-alcoholic steatohepatitis. Cochrane Database Syst Rev 2013;12:CD008623.
31. Tamburini BAJ, Finlon JM, Gillen AE, Kriss MS, Riemondy KA, Fu R, Schuyler RP, Hesselberth JR, Rosen HR, Burchill MA. Chronic liver disease in humans

causes expansion and differentiation of liver lymphatic endothelial cells. Front Immunol 2019;10:1036.
32. McGettigan B, McMahan R, Orlicky D, Burchill M, Danhorn T, Francis P, Cheng LL, Golden-Mason L, Jakubzick CV, Rosen HR. Dietary lipids differentially shape nonalcoholic steatohepatitis progression and the transcriptome of Kupffer cells and infiltrating macrophages. Hepatology 2019;70:67–83.
33. McCullough RL, McMullen MR, Poulsen KL, Kim A, Medof ME, Nagy LE. Anaphylatoxin receptors C3aR and C5aR1 are important factors that influence the impact of ethanol on the adipose secretome. Front Immunol 2018;9:2133.
34. Zhang F, Zarkada G, Han J, Li J, Dubrac A, Ola R, Genet G, Boye K, Michon P, Kunzel SE, Camporez JP, Singh AK, Fong GH, Simons M, Tso P, Fernandez-Hernando C, Shulman GI, Sessa WC, Eichmann A. Lacteal junction zippering protects against diet-induced obesity. Science 2018;361:599–603.
35. Feng J, Han J, Pearce SF, Silverstein RL, Gotto AM Jr, Hajjar DP, Nicholson AC. Induction of CD36 expression by oxidized LDL and IL-4 by a common signaling pathway dependent on protein kinase C and PPAR-gamma. J Lipid Res 2000;41:688–696.
36. Huggenberger R, Siddiqui SS, Brander D, Ullmann S, Zimmermann K, Antsiferova M, Werner S, Alitalo K, Detmar M. An important role of lymphatic vessel activation in limiting acute inflammation. Blood 2011;117:4667–4678.
37. Srinivasan RS, Escobedo N, Yang Y, Interiano A, Dillard ME, Finkelstein D, Mukatira S, Gil HJ, Nurmi H, Alitalo K, Oliver G. The Prox1-Vegfr3 feedback loop maintains the identity and the number of lymphatic endothelial cell progenitors. Genes Dev 2014;28:2175–2187.
38. Hong YK, Harvey N, Noh YH, Schacht V, Hirakawa S, Detmar M, Oliver G. Prox1 is a master control gene in the program specifying lymphatic endothelial cell fate. Dev Dyn 2002;225:351–357.
39. Breslin JW, Gaudreault N, Watson KD, Reynoso R, Yuan SY, Wu MH. Vascular endothelial growth factor-C stimulates the lymphatic pump by a VEGF receptor-3-dependent mechanism. Am J Physiol Heart Circ Physiol 2007;293:H709–H718.
40. Makinen T, Veikkola T, Mustjoki S, Karpanen T, Catimel B, Nice EC, Wise L, Mercer A, Kowalski H, Kerjaschki D, Stacker SA, Achen MG, Alitalo K. Isolated lymphatic endothelial cells transduce growth, survival and migratory signals via the VEGF-C/D receptor VEGFR-3. EMBO J 2001;20:4762–4773.
41. Ding BS, Nolan DJ, Butler JM, James D, Babazadeh AO, Rosenwaks Z, Mittal V, Kobayashi H, Shido K, Lyden D, Sato TN, Rabbany SY, Rafii S. Inductive angiocrine signals from sinusoidal endothelium are required for liver regeneration. Nature 2010;468:310–315.
42. Nakamoto S, Ito Y, Nishizawa N, Goto T, Kojo K, Kumamoto Y, Watanabe M, Majima M. Lymphangiogenesis and accumulation of reparative macrophages contribute to liver repair after hepatic ischemia-reperfusion injury. Angiogenesis 2020;23:395–410.
43. Zheng M, Yu J, Tian Z. Characterization of the liver-draining lymph nodes in mice and their role in mounting regional immunity to HBV. Cell Mol Immunol 2013;10:143–150.
44. Rajman I, Eacho PI, Chowienczyk PJ, Ritter JM. LDL particle size: an important drug target? Br J Clin Pharmacol 1999;48:125–133.
45. Wong BW, Wang X, Zecchin A, Thienpont B, Cornelissen I, Kalucka J, Garcia-Caballero M, Missiaen R, Huang H, Bruning U, Blacher S, Vinckier S, Goveia J, Knobloch M, Zhao H, Dierkes C, Shi C, Hagerling R, Moral-Darde V, Wyns S, Lippens M, Jessberger S, Fendt SM, Luttun A, Noel A, Kiefer F, Ghesquiere B, Moons L, Schoonjans L, Dewerchin M, Eelen G, Lambrechts D, Carmeliet P. The role of fatty acid beta-oxidation in lymphangiogenesis. Nature 2017;542:49–54.
46. Cromer WE, Zawieja SD, Tharakan B, Childs EW, Newell MK, Zawieja DC. The effects of inflammatory cytokines on lymphatic endothelial barrier function. Angiogenesis 2014;17:395–406.
47. Franchitto A, Onori P, Renzi A, Carpino G, Mancinelli R, Alvaro D, Gaudio E. Expression of vascular endothelial growth factors and their receptors by hepatic progenitor cells in human liver diseases. Hepatobiliary Surg Nutr 2013;2:68–77.
48. Witte MH, Dumont AE, Cole WR, Witte CL, Kintner K. Lymph circulation in hepatic cirrhosis: effect of portacaval shunt. Ann Intern Med 1969;70:303–310.
49. Schwager S, Renner S, Hemmerle T, Karaman S, Proulx ST, Fetz R, Golding-Ochsenbein AM, Probst P, Halin C, Neri D, Detmar M. Antibody-mediated delivery of VEGF-C potently reduces chronic skin inflammation. JCI Insight 2018;3:e124850.
50. Lammoglia GM, Van Zandt CE, Galvan DX, Orozco JL, Dellinger MT, Rutkowski JM. Hyperplasia, de novo lymphangiogenesis, and lymphatic regression in mice with tissue-specific, inducible overexpression of murine VEGF-D. Am J Physiol Heart Circ Physiol 2016;311:H384–H394.
51. Henri O, Pouehe C, Houssari M, Galas L, Nicol L, Edwards-Levy F, Henry JP, Dumesnil A, Boukhalfa I, Banquet S, Schapman D, Thuillez C, Richard V, Mulder P, Brakenhielm E. Selective stimulation of cardiac lymphangiogenesis reduces myocardial edema and fibrosis leading to improved cardiac function following myocardial infarction. Circulation 2016;133:1484–1497; discussion 1497.
52. Hasegawa S, Nakano T, Torisu K, Tsuchimoto A, Eriguchi M, Haruyama N, Masutani K, Tsuruya K, Kitazono T. Vascular endothelial growth factor-C ameliorates renal interstitial fibrosis through lymphangiogenesis in mouse unilateral ureteral obstruction. Lab Invest 2017;97:1439–1452.
53. Lanaspa MA, Andres-Hernando A, Orlicky DJ, Cicerchi C, Jang C, Li N, Milagres T, Kuwabara M, Wempe MF, Rabinowitz JD, Johnson RJ, Tolan DR. Ketohexokinase C blockade ameliorates fructose-induced metabolic dysfunction in fructose-sensitive mice. J Clin Invest 2018;128:2226–2238.

54. Finlon JM, Burchill MA, Tamburini BAJ. Digestion of the murine liver for a flow cytometric analysis of lymphatic endothelial cells. J Vis Exp 2019;143, 10.3791/58621.
55. Fu R, Gillen AE, Sheridan RM, Tian C, Daya M, Hao Y, Hesselberth JR, Riemondy KA. clustifyr: an R package for automated single-cell RNA sequencing cluster classification. F1000Res 2020;9:223.
56. Nemkov T, Reisz JA, Gehrke S, Hansen KC, D'Alessandro A. High-throughput metabolomics: isocratic and gradient mass spectrometry-based methods. Methods Mol Biol 2019;1978:13–26.
57. Faul F, Erdfelder E, Lang AG, Buchner A. G*Power 3: a flexible statistical power analysis program for the social, behavioral, and biomedical sciences. Behav Res Methods 2007;39:175–191.
58. Kim HY. Statistical notes for clinical researchers: sample size calculation 1. comparison of two independent sample means. Restor Dent Endod 2016; 41:74–78.

Received April 28, 2020. Accepted September 16, 2020.

Correspondence Address correspondence to: Matthew A. Burchill, PhD, University of Colorado Anschutz Medical Campus, Department of Medicine, Division of Gastroenterology and Hepatology, 12700 East 19th Avenue, P15-10119, Aurora, Colorado 80045. Fax: (303) 724-7243. e-mail: matthew.burchill@cuanschutz.edu; or Beth A. Jirón Tamburini, PhD, University of Colorado Anschutz Medical Campus, Department of Medicine, Division of Gastroenterology and Hepatology, 12700 East 19th Avenue, P15-10122, Aurora, Colorado 80045. Fax: 303-724-7243. e-mail: beth.tamburini@cuanschutz.edu.

Acknowledgments
The authors thank Erin Kitten, Kim Jordan, and Angie Minic and the University of Colorado Anschutz Human Immunology Shared Resource for assistance with flow sorting and Vectra image acquisition. They also thank Rachael Dran and Veronica Wessells for assistance in processing human tissue for pathology. Finally, the authors thank Erin Lucas and Thu Doan for critical review of the manuscript.

CRediT Authorship Contributions

Matthew Alan Burchill (Conceptualization: Lead; Data curation: Equal; Formal analysis: Equal; Funding acquisition: Supporting; Investigation: Equal; Methodology: Lead; Project administration: Equal; Resources: Supporting; Supervision: Supporting; Writing – original draft: Equal; Writing – review & editing: Equal)

Jeffrey M. Finlon (Data curation: Supporting; Formal analysis: Supporting; Investigation: Supporting; Writing – review & editing: Equal)

Alyssa R. Goldberg (Conceptualization: Supporting; Data curation: Supporting; Formal analysis: Supporting; Writing – original draft: Supporting; Writing – review & editing: Supporting)

Austin E. Gillen (Data curation: Equal; Formal analysis: Equal; Methodology: Equal; Software: Lead; Writing – review & editing: Supporting)

Petra A. Dahms (Data curation: Supporting; Formal analysis: Supporting)

Rachel H. McMahan (Conceptualization: Supporting; Data curation: Supporting)

Anne Tye (Data curation: Supporting; Formal analysis: Supporting; Methodology: Supporting)

Andrew B. Winter (Data curation: Supporting; Formal analysis: Supporting)

Julie A. Reisz (Data curation: Supporting; Formal analysis: Supporting; Writing – review & editing: Equal)

Eric Bohrnsen (Data curation: Supporting; Formal analysis: Supporting)

Johnathon B. Schafer (Data curation: Supporting; Formal analysis: Supporting; Writing – review & editing: Supporting)

Angelo D'Alessandro (Supervision: Supporting; Writing – review & editing: Supporting)

David J. Orlicky (Formal analysis: Supporting; Methodology: Supporting; Writing – review & editing: Supporting)

Michael S. Kriss (Conceptualization: Supporting; Writing – review & editing: Supporting)

Hugo R. Rosen (Supervision: Supporting; Writing – review & editing: Supporting)

Rebecca L. McCullough (Conceptualization: Supporting; Data curation: Supporting; Investigation: Supporting; Project administration: Supporting; Supervision: Supporting; Writing – review & editing: Equal)

Beth A. Tamburini (Conceptualization: Lead; Data curation: Lead; Formal analysis: Lead; Funding acquisition: Lead; Investigation: Lead; Supervision: Lead; Writing – original draft: Lead; Writing – review & editing: Lead)

Conflicts of Interest
The authors disclose no conflicts.

Funding
Matthew A. Burchill is supported by funding through the University of Colorado Anschutz GI and Liver Innate Immune Program Pilot award and Linda Crnic Institute Grand Challenge Pilot. Alyssa R. Goldberg is supported by the Ruth L. Kirschstein National Research Service Award Institutional Research Training Grant T32 DK067009. Anne Tye is supported by funding through the University of Colorado Anschutz Consortium for Fibrosis Research and Translation postdoctoral fellowship. Johnathon B. Schafer is supported by University of Colorado Anschutz Molecular Biology Graduate Program T32 supplement GM008730-20S1. Rebecca L. McCullough is supported by National Institutes of Health R00 AA025386. Beth A. Jirón Tamburini is funded by National Institutes of Health R01 AI121209 and the University of Colorado Outstanding Early Career Scholar and RNA Biosciences Initiative Clinical Scholar Award. Beth A. Jirón Tamburini and Matthew A. Burchill are also supported by the Waterman Family Foundation for Liver Research and National Institutes of Health DK125595.